Journal of
Water & Climate Change

IWA PUBLISHING

Journal of Water and Climate Change Vol 13 No 9, 3274 doi: 10.2166/wcc.2022.089

Performance assessment of interpolation techniques for optimal areal rainfall–temperature estimation: the case of two contrasting river catchments, Akaki and Mille, in Ethiopia

Hirpo Gudeta Bati [a,*], Tenalem Ayenew Tegaye[b] and Tena Alemirew Agumassie[c]

[a] Africa Center of Excellence for Water Management, Addis Ababa University, Addis Ababa, Ethiopia
[b] School of Earth Sciences, Addis Ababa University, Addis Ababa, Ethiopia
[c] Ethiopian Institute of Water Resources, Addis Ababa University, Addis Ababa, Ethiopia
*Corresponding author. E-mail: hirpo.gudeta@aau.edu.et

HGB, 0000-0003-1885-0487

ABSTRACT

In the topographic complex catchments, landscape features have a significant impact on the spatial prediction of rainfall and temperature. In this study, performance assessments were made of various interpolation techniques for the prediction of the spatial distribution of rainfall and temperature in the Mille and Akaki River catchments, Ethiopia, through an improved approach on selecting the auxiliary variables as a covariate. Two geostatistical interpolation techniques, ordinary kriging (OK) and kriging with external drift (KED), and one deterministic interpolation technique, inverse distance weighting (IDW), were tested through a leave-one-out cross-validation (LOOCV) procedure. The results indicated that using the multivariate geostatistical interpolation technique (KED) with the auxiliary variables as a covsariate outperformed the univariate geostatistical (OK) and deterministic (IDW) techniques for the spatial interpolation of sampled rainfall–temperature data in both contrasting catchments, Akaki and Mille, with the lowest estimation errors (e.g., for Mille annual mean rainfall: root mean square error=75.32, 77.34, 245.72, mean bias error=3.70, −33.18, −15.61, mean absolute error=67.99, 69.51, 192.64) using KED with the combination of elevation and easting as a covariate, IDW and OK, respectively. Thus, the study confirmed that the use of elevation and easting/northing coordinates as predictors in geostatistical interpolation techniques could significantly improve the spatial prediction of climatic variables.

Key words: cross-validation, deterministic Interpolation, geostatistical interpolation, variogram

HIGHLIGHTS

- Globally, there is no suitable interpolation technique for the spatial prediction of climatic variables like rainfall and temperature.
- In the mountainous catchment, geostatistical interpolation outperforms deterministic interpolation techniques.
- The combination of elevation and easting as a covariate significantly improves the performance of the spatial prediction of climatic variables.

GRAPHICAL ABSTRACT

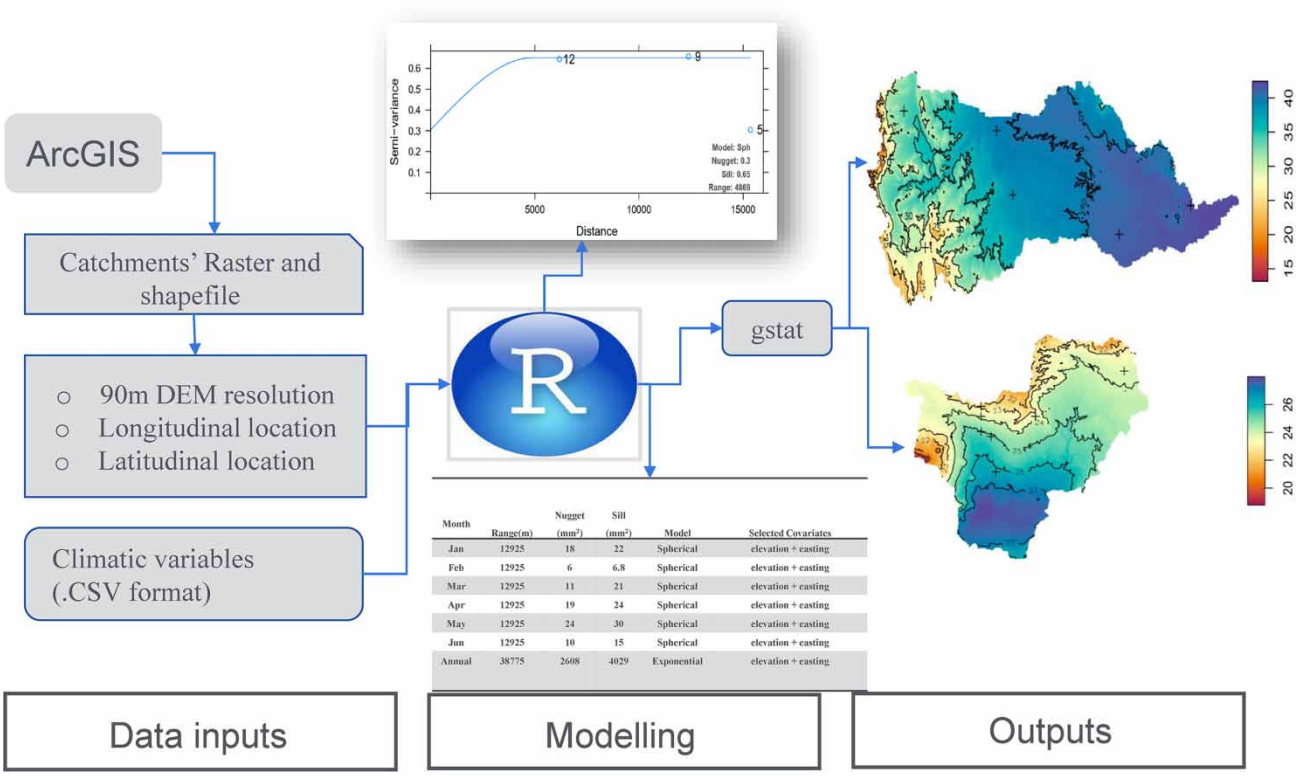

1. INTRODUCTION

In the topographic complex catchments, optimum spatial predictions of climatic variables, specifically rainfall and temperature, are essential as a principal input for downstream applications, namely hydrological and/or hydraulic modeling (Lebel *et al.* 1987; Grimes *et al.* 1999), flood early warning, forecasting, and drought management (Bertini *et al.* 2020; Lu *et al.* 2020). However, in developing countries, the spatial array of the weather stations of the aforementioned input rainfall and temperature is irregular and highly sparse, and the low network density (Washington *et al.* 2006; Parker *et al.* 2011; Dinku 2019) in Ethiopia is not exceptional.

In Ethiopia, specifically in the lowlands, the spatial coverage of weather stations is highly sparse, and they are below the standard of the World Meteorological Organization (WMO) (Washington *et al.* 2006; Dinku *et al.* 2017).

Although historically the ground-based stations have been the key source of rainfall and temperature for catchments' spatial pattern prediction and areal mean estimation (Taesombat & Sriwongsitanon 2009; Ly *et al.* 2011; Di Piazza *et al.* 2015; Adhikary *et al.* 2017), the satellite-based climate data have been taking a leading role in predicting areal mean products, especially rainfall and temperature using different prediction algorithms based on the satellite imagery, mainly geostationary satellites, i.e. Meteosat Second Generation (MSG-2), which can produce high imagery both at spatial and temporal resolutions (Gebremichael & Hossain 2010; Gebere *et al.* 2015; Chen & Li 2016).

Although satellite-based weather data take advantage of ground-based highly sparse gauged weather data in many aspects, for instance covering a large area at different spatial and temporal scales, there are still some limitations to using satellite-based climatic data alone. For example, since the precipitation measurement is indirect, the accuracy is less, which requires calibrations using ground-based rainfall data, specifically over mountainous regions (Dinku *et al.* 2008b), and tends to underestimate high rainfall values in mountainous regions such as Ethiopia (Le Coz & Van De Giesen 2020) and overestimate low rainfall events (Toté *et al.* 2015). In addition to the aforementioned limitations, the spectral resolution of sensors, such as thermal infrared (TIR) and passive micro-wave (PMW), varies with wavelength and fails to capture more accurate images and predictions of climate variability. For instance, PMW sensors cannot properly capture and identify very cold cloud-based rainfall from ice, especially at the top of mountainous regions, and background emissions from the land surface,

which vary significantly depending on landscape characteristics (Toté *et al.* 2015; Petković & Kummerow 2017). Distinguishing raining clouds from the non-raining cloud, like Cirrus clouds from top cloud temperature, and being unable to detect warm orographic rainfall are some limitations of TIR sensors (Dinku *et al.* 2008a).

A novel approach, which is blending satellite and ground-based climatic data for optimum areal mean climatic variable estimation, has emerged for three decades to solve the aforementioned limitations (Grimes *et al.* 1999; Yang *et al.* 2017; Dinku *et al.* 2017; Gebremedhin *et al.* 2021).

There are two types of interpolation methods: deterministic interpolation methods, for example, radial basis function (RBF) (Yang *et al.* 2017) and inverse distance weighting (IDW) (Goovaerts 2000), and geostatistical interpolation methods such as simple kriging (SK), ordinary kriging (OK), ordinary cokriging (CK), universal kriging (UK), and kriging with external drift (KED) (Phillips *et al.* 1992; Goovaerts 2000; Haberlandt 2007; Taesombat & Sriwongsitanon 2009; Ly *et al.* 2011; Mukhopadhaya 2016).

Novikov (1981) investigated the impact of elevation on the prediction of the spatial pattern of precipitation and temperature for the New Hampshire and Vermont mountainous catchment via simple linear regression, and the results indicated that the mean monthly precipitation increases strongly with elevation, whereas the mean monthly temperature decreases with elevation. Cantet (2017) compared several spatial interpolation techniques to map the mean annual and monthly precipitation of a small island, which has a complex topography, and the results indicated that the KED seems to outperform regression methods. Similarly, another study in which the dependency of monthly precipitation on elevation was analyzed by Lloyd (2005), focusing on Great Britain through the comparison of different interpolation techniques, concluded that KED with an elevation as a covariate provides the most accurate estimates of precipitation for most months. Hudson & Wackernagel (1994) noted that the integration of information about elevation as a covariate into the mapping of temperature by kriging improves the performance of prediction. Numerous scholars have used the comparison approach of different interpolation methods to predict the spatial disparity of rainfall and groundwater depth (Kisaka *et al.* 2016; Adhikary & Dash 2017; Amini *et al.* 2019; Jalili Pirani & Modarres 2020), and their results indicated that geostatistical interpolation techniques yield more accurate predictions than deterministic techniques.

The aforementioned literature review indicated that there was no globally suitable interpolation technique, and thus while scholars used a comparative approach to assess the performance and select the suitable method for a specific site and a specific objective, and as a knowledge gap, none of them considered the effect of the combination of elevation and easting or northing as a covariate on the spatial prediction of climatic variables. Therefore, this research aimed (i) to assess the performance of the deterministic model (IDW) and two geostatistical models, OK and KED interpolation techniques, and (ii) to select and use the suitable technique for contrasting catchments, Mille and Akaki's climatic variable spatial pattern prediction, based on statistical and graphical evaluation methods.

2. MATERIAL AND METHODS

2.1. Study area

This research paper considers two contrasting catchments (in terms of physiographic features like climatic condition and land cover) in the Awash River Basin as the case study area, namely the Mille River catchment and the Akaki River catchment, which are located in the Western escarpment and the upper part of the Awash River Basin, respectively (Figure 1).

The Mille River catchment is situated between 39 °5′ and 40 °9′ longitude and 11 °2′ and 11 °8′ latitude, and covers an area of 5,598.74 km^2. Water resource management is an essential issue in the Mille River catchment because of its wide range of water uses in its upper part as well as its lower part user requirements and environmental flow provisions (Ministry of Water Resources 2009). The catchment significantly contributes to the water supply for different purposes like irrigation to communities that reside within it, specifically communities living in the upper catchment (Ministry of Water Resources 2009), and it contributes a considerable share to the Tendaho multipurpose reservoir inflows. Consequently, a more accurate spatial distribution of rainfall in the whole catchment, particularly the upper part, would be essential for downstream water resource management and developments, including Tendaho Reservoir operation.

The topography of the catchment is characterized by steep slopes of ridges and mountains in the upper part to a gentle slope in the low-lying part.

The annual rainfall average in the Mille catchment ranges from 374.2 to 1,032 mm, with the highest and lowest monthly average in August and February, respectively (Figure 2). The maximum and minimum mean temperatures range from 28.820 to 43.210 °C and 10.270 to 18.980 °C, respectively.

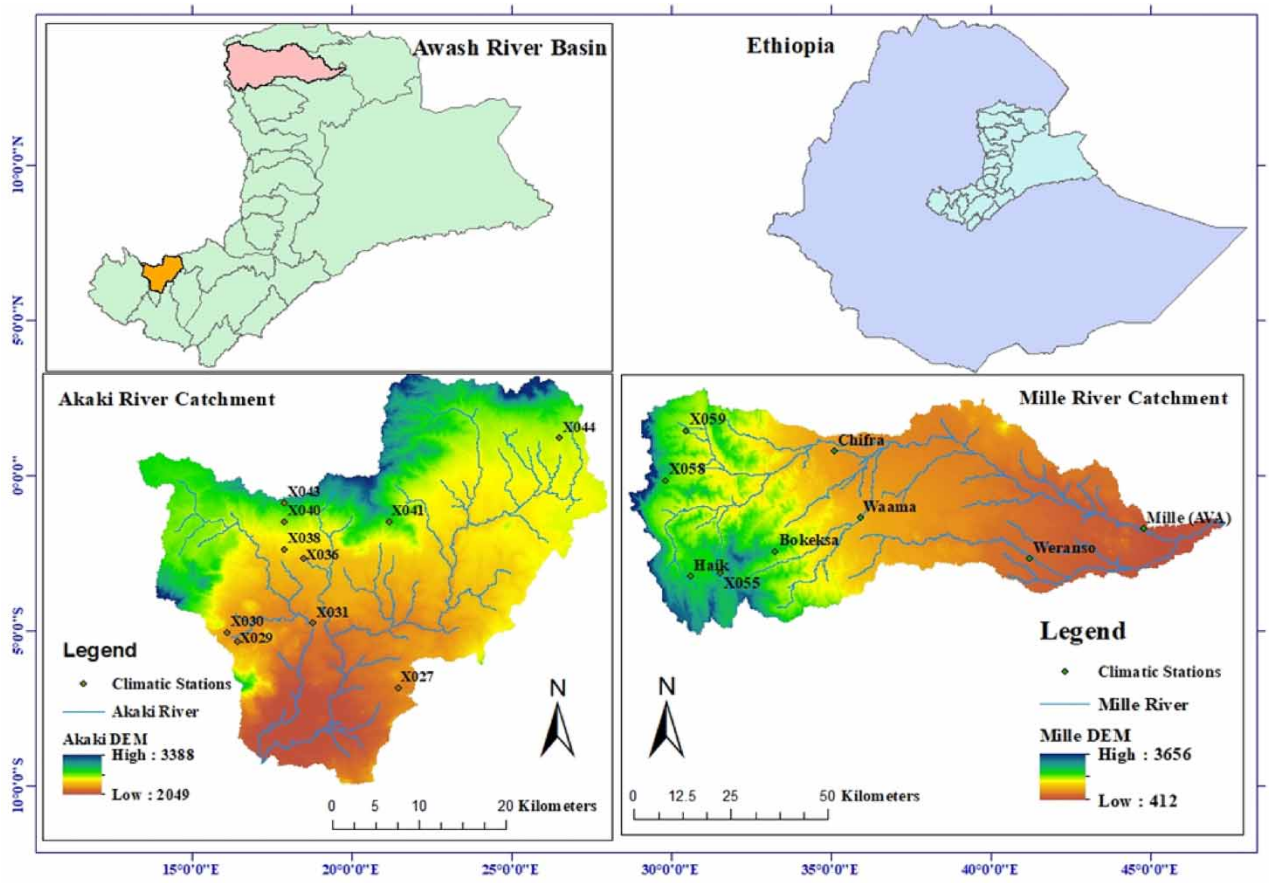

Figure 1 | Location of the study area.

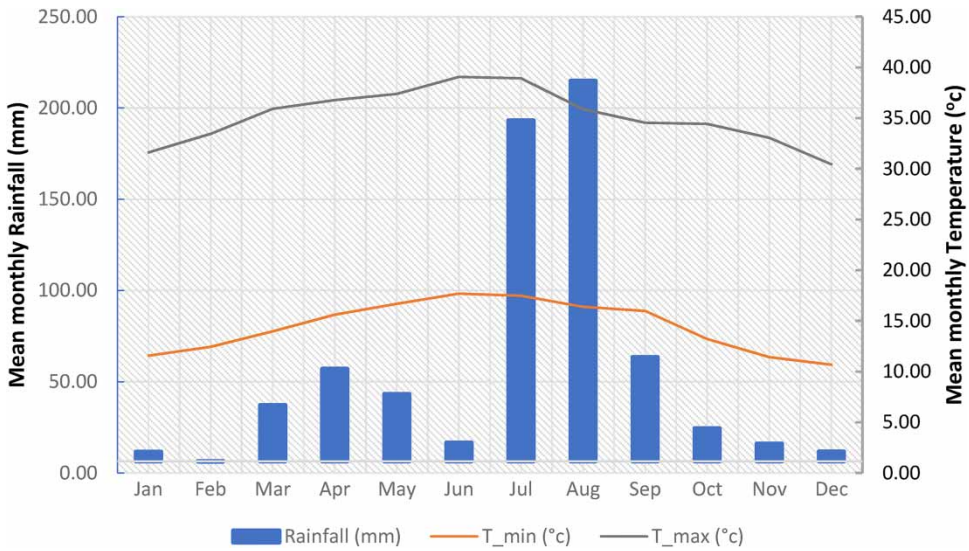

Figure 2 | Mille catchment's mean monthly climatological variables.

The Akaki River catchment is located in the northwestern escarpment of the Awash River Basin, Ethiopia, and covers an area of about 1,425 km^2. It is located between 38 °6′ and 39 °1′ longitude and 8 °8′ and 9 °2′ latitude (see Figure 1). The Akaki catchment is circumscribed by the Intoto Mountains to the north, Mount Menagesha and Wechecha volcanic mountains to

the west, and Yerer Mountain to the east. In the Akaki catchment, there are three surface water reservoirs, Legedadi, Dire, and Gefersa Reservoir, which are used for water supply for Addis Ababa city and its surrounding towns, and one hydropower reservoir, Abasamuel. The catchment is very important from a water supply point of view, specifically for Addis Ababa and its surrounding communities and for agricultural production.

The climate of the Akaki catchment has two distinct wet seasonal weather patterns. The main rainy season starts from late June to mid-September, which contributes almost 70% of the total annual rainfall, and the pre-rainy season starts from March to mid-May (Molla *et al.* 2005). Based on historic climatic data (2000–2016), the mean minimum and maximum rainfall was 935.2 and 1,011.6 mm, respectively. The mean minimum and maximum annual temperatures of the catchment vary from 8.640 to 10.330 °C and 21.610 to 23.460 °C, respectively (Figure 3).

2.2. Datasets

Both historic ground-based point data and blended gridded climatic variables, specifically rainfall and temperature data, were obtained from the National Meteorological Agency (NMA), Ethiopia, from 1 January 1983 to 31 December 2016 (Table 1 and Figure 1). The blended pixel climatic dataset was merged from the European Meteorological Satellites (METEOSAT) and ground-based observations at the national level for some African nations, including Ethiopia (Dinku *et al.* 2017). However, the ground-based climatic datasets were missing climatic variable values on some consecutive days, months, and years (>10% missing data) for most ground stations. As a solution, we took a blended pixel value of the grid in which the gauging station

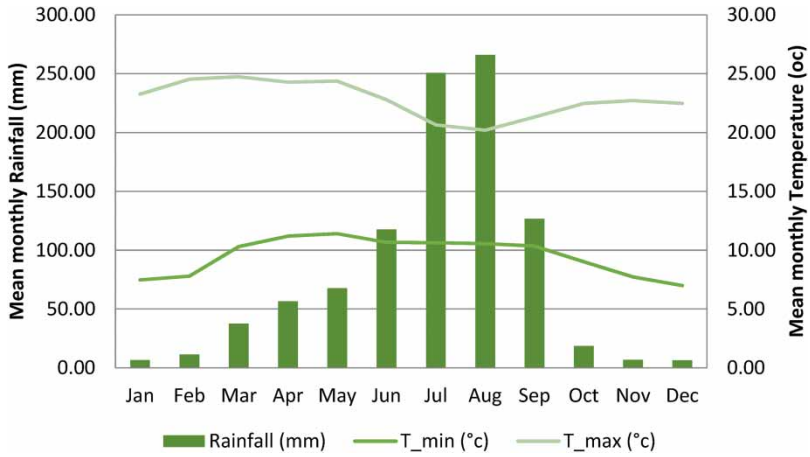

Figure 3 | Akaki catchment's mean monthly climatological variables.

Table 1 | Mille and Akaki catchments' climatological stations

Mille catchment				Akaki catchment			
Stations	**Altitude (m.a.s.l)**	**Longitude**	**Latitude**	**Stations**	**Altitude (m.a.s.l)**	**Longitude**	**Latitude**
X055	2,089	39.75	11.32	**X027**	2,202	38.85	8.88
X058	1,854	40.77	11.43	**X029**	2,279	38.68	8.93
X059	1,573	39.62	11.54	**X030**	2,282	38.67	8.94
Weranso	643	39.67	11.66	**X031**	2,197	38.76	8.95
Waama	1,020	39.61	11.75	**X036**	2,385	38.75	9.02
Mille (AVA)	491	40.48	11.35	**X038**	2,440	38.73	9.03
Haik	2,003	40.08	11.45	**X040**	2,606	38.73	9.06
Chifra	928	40.00	11.75	**X041**	2,741	38.84	9.06
Bokeksa	1,771	40.75	11.42	**X043**	2,771	38.73	9.08
				X044	2,543	39.02	9.15

was laid within it, and then the authors performed the correlation and regression analysis (not shown here) with ground-based historic climate datasets to check the similarity between two neighboring sample climatic datasets. We obtained that a pixel value of a grid was much more strongly correlated with ground-based historic climate data because of the close sample distance, and the same result was confirmed by Wilson *et al.* (1998). Therefore, based on their correlation, we selected and used pixel values as point data instead of gauged station data. As a consequence, we selected and used nine pixel values for the Mille catchment and 10 pixel values for the Akaki catchment as the point station dataset, which were used as principal variables for spatial pattern prediction using different interpolation techniques. Based on collected daily data, monthly and annual data for climatological variables were developed to predict the spatial pattern of both the rainfall and temperature of the interesting study areas, the Mille and Akaki catchments.

Unlike deterministic and univariate geostatistical interpolation techniques, multivariate geostatistical interpolation methods, for instance KED, account for secondary information in the prediction of spatial climatological variables. The 90 m spatial resolution digital elevation model (DEM) elevation, longitudinal, and latitudinal positions, and their combination were considered as auxiliary variables (covariates) in this study.

In this research, the integration of R-programming with the gstat package (Pebesma 2004, 2012) and GIS tools were applied for spatiotemporal interpolation techniques, preprocessing raster layers containing the predictive variables, and preparing shapefiles.

2.3. Methods

The three stages followed in the study plan were (1) the preparation and export of monthly and annual climatic variable data in '.csv' format, exporting raster of DEM, easting, and northing, and shapefiles for catchments into R-programming, (2) various interpolation technique applications to generate a spatial pattern of rainfall and temperature map and to estimate areal mean rainfall and temperature (minimum and maximum), and (3) the assessment of the performance of various interpolation methods based on statistical evaluation criteria. The details of each step are described as follows.

2.3.1. Collection and preprocessing of sampled historical climatological datasets

The sampled historic climatic data were collected and processed as Excel spreadsheets, and they were prepared and exported in '.csv' format for monthly and annual rainfall and temperature. Consequently, the prepared sampled data were exported into R-programming for the various types of spatial interpolation techniques. Simultaneously, the sampled data location shapefiles, elevation, latitudinal, longitudinal raster, and shapefile of the study area were imported into R-programming. In R-programming, point data were converted to a spatial points data frame (SPDF) using a longitude and latitude coordinate system. Then, for better work in R, the longitudinal–latitudinal coordinate system was transformed to the Universal Transverse Mercator (UTM) coordinate system. Finally, the sampled climatic data were combined with location data to form a new spatial point data frame.

2.3.2. Interpolation techniques

Various spatial interpolation techniques used in this study were briefly introduced and compared in R-programming (https://cran.r-project.org) through gstat (Pebesma & Wesseling 1998; Pebesma 2003) and related packages. For this study, based on their best performance (e.g., Chen & Liu 2012; Rata *et al.* 2020), one deterministic method, IDW, and two geostatistical methods, OK and KED, were selected among the various spatial interpolation techniques. For details of the description of geostatistical and other interpolation techniques, the reader can refer to geostatistical books (Wackernagel 1998, 2003; Webster & Oliver 2007).

2.3.2.1. Inverse distance weighting. The IDW method estimates values at ungauged/unsampled points by the weighted average of measured data that found surrounding points. It is based on the assumption that the sampled observations that are close to the estimated points have more weight control on the estimated value than the sampled observations far apart (Goovaerts 2000). According to Shepard (1968), the equation of IDW is given by:

$$Z_{\mathrm{IDW}}(U) = \sum_{\propto=1}^{n} \lambda(U_{\propto}) Z(U_{\propto})$$

$$\text{With} \quad \lambda(U_{\propto}) = \frac{(r_{\propto})^{-p}}{\sum_{\propto=1}^{n} (r_{\propto})^{-p}} \tag{1}$$

where $Z_{IDW}(U)$ is the climatic variable (in our case, either rainfall or temperature) at the unsampled point (U), $Z(U_\propto)$ is the climatic variable at the sampled location $U_\propto$, $\propto = 1,\ 2,\ \ldots, n$, and $\lambda(U_\propto)$ are the undetermined weights to be estimated as a function of distance.

The inverse distance power (p) by default is 2 (Shepard 1968; Goovaerts 2000; Otieno *et al.* 2014). However, the authors took a certain value of inverse distance power (Table 2) in an interval of one unit to test the performance of each power and selected the best power using the LOOCV method. Accordingly, power 4 was selected for the Mille catchment, and power 3 was selected for the Akaki catchment.

2.3.2.2. Ordinary kriging. Ordinary kriging (OK) is one of the geostatistical interpolation techniques by which local variation is considered by limiting the domain of stationarity of the unknown local mean $(m(X))$ to the local neighborhood, and the kriging weights sum to one (Goovaerts 1997, 2000; Webster & Oliver 2007). Its equation is given by:

$$Z_{OK}(X) = \sum_{\propto=1}^{n} (\lambda)^{OK}(X_\propto) Z(X_\propto) + \left[1 - \sum_{\propto=1}^{n} \lambda^{OK}(X_\propto)\right] m(X)$$

$$Z_{OK}(X) = \sum_{\propto=1}^{n} (\lambda)^{OK}(X_\propto) Z(X_\propto) \qquad (2)$$

$$\text{With} \quad \sum_{\propto=1}^{n} \lambda^{OK}(X_\propto) = 1$$

where $Z_{OK}(X)$ is the climatic variable (in our case, rainfall and temperature) predicted at the unknown location (X) using the OK method, $Z(X_\propto)$ are the sampled values at $X_\propto$'s n data locations, and $\lambda^{OK}(X_\propto)$ are the OK weights determined to minimize the estimation of variance while confirming no biasedness of the OK estimator (Goovaerts 1997; Wackernagel 1998). It is mathematically expressed as follows:

$$\delta^2 = \text{Var}\left[\{Z^*_{OK}(X_o) - Z(X_o)\}^2\right]$$

and the expected error is

$$\begin{aligned} E\{Z^*_{OK}(X_o) - Z(X_o)\} &= E\left[\sum_{\propto=1}^{N} \lambda_\propto Z(X_\propto) - Z(X_O) \sum_{\propto=1}^{N} \lambda_\propto\right] \\ &= \sum_{\propto=1}^{n} \lambda_\propto E[Z(X_\propto) - Z(X_O)] \\ &= 0 \end{aligned} \qquad (3)$$

Table 2 | Inverse distance power selection using the LOOCV method (for the month of January)

Idp = *n*, where *n* = 1, 2, 3, 4, 5, 6	RMSE	
	Mille catchment	Akaki catchment
1	5.153	1.274
2	4.353	1.221
3	3.940	1.206
4	3.861	1.210
5	3.900	1.219
6	3.960	1.226

According to Goovaerts (1997, 2000), the weights are acquired by solving a system of linear equations known as the 'OK system', which is given by the following equation:

$$\begin{cases} \sum_{\beta=1}^{n} \lambda_\beta(X)\gamma(X_\alpha - X_\beta) - \mu(X) = \gamma(X_\alpha - X_o), & \alpha = 1 \ldots n \\ \sum_{\beta=1}^{n} \lambda_\beta(X) = 1 \end{cases} \tag{4}$$

where $\mu(X)$ is the Lagrange parameter.

Unlike IDW, any geostatistical technique such as OK uses a variogram but not Euclidean distance to measure the degree of dissimilarity between sampled data $Z(U_\alpha)$ and unsampled value $Z(U_O)$ (Goovaerts 2000; Webster & Oliver 2007). Let two distinct climatic data values $Z\ (U_\alpha)$ and $Z\ (U_\alpha + h)$ at two different locations be given, and if we assume isotropy, which is the direction independence of the semi-variance, then the more distant sample value should receive less weight in the estimation of $Z\ (U_o)$. The experimental variogram is calculated as half the average squared difference between the components of value pairs, as presented in Equation (5) and described in Goovaerts (2000):

$$\hat{\gamma}(h) = \frac{1}{2N(h)} \sum_{\alpha=1}^{N(h)} [Z(U_\alpha + h) - Z(U_\alpha)]^2 \tag{5}$$

where $\hat{\gamma}(h)$ is the experimental variogram, which is a function of both the direction and the distance (anisotropic–spatial pattern), and $N\ (h)$ is the number of pairs of climatic variable data locations separated by lag distance/vector h.

In this study, the automap package automatically selects some models, namely spherical, exponential, and Ste Mat (Matern, M. Stein's parameterization) models, which are widely applied (Goovaerts 2000; Webster & Oliver 2007; Stein 2010; Frazier *et al.* 2016) to model the theoretical variogram.

The equations for the spherical, exponential, and Ste models are as follows:

$$\gamma(h) = \begin{cases} c_0 + c\left[\frac{3h}{2a} - \frac{1}{2}\left(\frac{h}{a}\right)^3\right] & \text{for } 0 < h \le a \\ c_0 + c & \text{for } h > a \\ 0 & \text{for } h = 0 \end{cases} \tag{6}$$

$$\gamma(h) = \begin{cases} c_0 + c\left[1 - \exp\left(-\frac{h}{a^*}\right)\right], & \text{for } 0 < h \\ 0 & \text{for } h = 0 \end{cases} \tag{7}$$

$$\gamma(h) = C\left\{1 - \frac{1}{2^{\nu-1}\Gamma(\nu)}\left(\frac{h}{r}\right)^{\nu} K_\nu\left(\frac{h}{r}\right)\right\} \quad \text{for } |h| > 0 \tag{8}$$

where c_0 is a nugget effect, c is the sill variance, h is the lag distance (m), a is the actual range, a^* is the practical range, which is three times ($a^* = 3a$) the actual range (Stein 2010), ν is the smoothness parameter varying from 0 to ∞, $\Gamma(.)$ is the gamma function, and $K_\nu(.)$ is the modified Bessel function.

The most common technique of fitting variogram models to compute experimental variograms is performed using manual fitting procedures (Nalder & Wein 1998; Haberlandt 2007). However, this is not an appropriate approach because it depends on the expertise and the sample size in the data (Ly *et al.* 2011). In this research paper, an automatic fitting procedure was applied using the '***autofitVariogram***' function from the package '***automap***' to choose the appropriate model for fitting a variogram model to an experimental variogram and also calibrated its parameters such as range, nugget, and sill.

2.3.2.3. Kriging with external drift. KED is a kind of universal kriging that replaces one or more variables as a predictor by the coordinates, and the trend mean, $m(u)$, is modeled as a linear function of smoothly varying covariates $y(u)$ instead of the spatial coordinates as a function (Goovaerts 1997; Webster & Oliver 2007):

$$\begin{aligned} & m(u) = a_o(u) + a_1(u)y(u) \\ & \text{With} \quad a_1(u) = \sum_{\infty=1}^{n} \lambda_\infty^{\text{KED}}(U)\ Z(u_\infty) \end{aligned} \tag{9}$$

where $m(u)$ is a local constant mean at location u, the trend coefficients a_o and a_1 are implicitly estimated through the kriging system within each search neighborhood $Z(u_\propto)$, and $y(u)$ is the independent variable used as an influence in the prediction of the dependent variable.

Let $y_1, y_2, y_3,\ldots,y_n$ be several independent (external) variables linearly related to $Z(u)$,

$$\begin{aligned} Z(u) &= \sum_{k=1}^{n} \beta_k y_k(u) + \varepsilon(u) \\ &= \beta_0 + \beta_1 y_1(u) + \beta_2 y_2(u) + \ldots + \beta_n y_n(u) + \varepsilon(u) \end{aligned} \tag{10}$$

and we might be able to calculate the KED estimator as follows:

$$\hat{Z}_{\mathrm{KED}}(X_0) = \sum_{\propto=1}^{n} \lambda_{\propto}^{\mathrm{KED}} Z(X_\propto) \tag{11}$$

The expectation is:

$$E[\hat{Z}_{\mathrm{KED}}(X_0)] = \sum_{k=1}^{K} \sum_{\propto=1}^{n} \beta_k \lambda_{\propto}^{\mathrm{KED}} y_k(X_\propto) \tag{12}$$

where β_k, $k = 1, 2, 3,\ldots,K$, are unknown coefficients to be determined, y_k are known external variables/covariates at location $X_\propto$, $\varepsilon(u)$ is the Lagrange multiplier, and $\lambda_{\propto}^{\mathrm{KED}}$ are kriging weights calculated by:

$$\begin{aligned} &\sum_{i=1}^{n} \lambda_i^{\mathrm{KED}} \gamma(X_i,\ X_j) + \varphi_0 + \sum_{k=1}^{K} \varphi_k y_k(X_j) = \gamma(X_0,\ Xj) \quad \text{for all } j = 1, 2, \ldots, n, \\ &\sum_{i=1}^{n} \lambda_i^{\mathrm{KED}} = 1 \end{aligned} \tag{13}$$

And the estimator is unbiased if:

$$\sum_{i=1}^{n} \lambda_i^{\mathrm{KED}} y_k(X_i) = y_k(X_0) \ \text{ for all } k = 1,\ 2,\ \ldots,\ K \tag{14}$$

where $\gamma(X_i,\ X_j)$ is the semi-variance between the data points X_i and X_j, $\gamma(X_0,\ X_j)$ is the semi-variance between the target point and the data points surrounding the estimated point, and φ_0 and φ_k, $k = 1, 2,\ldots,K$ is a Lagrange multiplier.

Among spatial interpolation methods, the geostatistical technique assumes that the variable is normally distributed (Isaaks & Srivastava 1989). However, point data is/are often not symmetrical (skewness either to the right or to the left), which affects spatial reduction of input data in which the few values will overcome all the others. According to Goovaerts (1997), nonsymmetrical distributions are often transformed to conditions of normality using one of the three transformations such as natural logarithmic function, square root transformation to reduce the skewness of input data, and the influence of extreme values. But, for small sampled data such as our case, we have chosen not to use transformation to conditions of normality for the sake of highly sparsely distributed gridded sampled climate data (Rossiter 2014; Bati 2022), and we have also intended to ignore the possibility of anisotropy for this research work for the sake of not missing the remaining sample data and for simplicity of modeling.

2.3.3. Performance evaluation

The performances of three selected interpolation techniques, IDW, OK, and KED, were accomplished via evaluations and comparisons of estimated climatic variable values and observed data. In this study, the available climatic variable data were split into two parts: training and test/validation data. The training data were used to fit the model, while the test data were used to calculate prediction accuracy, and the procedure is called regular-validation.

The cross-validation procedure was applied to compare the spatial interpolation performance of KED with univariate interpolation methods. The basic idea behind cross-validation is that we split our test/validation dataset into k-folds. For this study, the commonly used type of cross-validation, the so-called leave-one-out cross-validation (LOOCV), was applied, where the climatic data consecutively took the role of test data, and the remaining data took the role of training data. We train our model on $k-1$ folds and use the resulting model to predict the values of the left-out fold. In our case, sampled climatic data for two contrasting catchments, Mille (number of observations ($k=9$)) and Akaki (number of observations ($k=10$)), from 2000 to 2016 were used for modeling. Accordingly, the LOOCV technique involves using only one observation data as the test set and the $k-1$ remaining observations as the training set.

To assess and select a suitable interpolation technique, this study evaluated and compared different interpolation techniques via four statistical indicators, such as root mean square error (RMSE), mean bias error (MBE), mean absolute error (MAE), and coefficient of correlation (r), between the predicted and observed climatic variable values, which are given as follows (Vicente-Serrano *et al.* 2003; Li & Heap 2008):

$$\text{RMSE} = \sqrt{\frac{1}{n}\sum_{i=1}^{n}\left(\hat{Z}(X_i) - Z(X_i)\right)^2} \tag{15}$$

$$\text{MBE} = \frac{1}{n}\sum_{i=1}^{n}\left[Z(X_i) - \widehat{Z}\,(X_i)\right] \tag{16}$$

$$\text{MAE} = \frac{1}{n}\sum_{i=1}^{n}\left[|\hat{Z}(X_i) - Z(X_i)|\right] \tag{17}$$

$$r = \frac{\sum_{i=1}^{n} Z(X_i) * \hat{Z}(X_i) - \left(\sum_{i=1}^{n} Z(X_i)\right)\left(\sum_{i=1}^{n} \hat{Z}(X_i)\right)}{\sqrt{n\left(\sum_{i=1}^{n}(Z(X_i))^2\right) - \left(\sum_{i=1}^{n} Z(X_i)\right)^2}\sqrt{n\left(\sum_{i=1}^{n}(\hat{Z}(X_i))^2\right) - \left(\sum_{i=1}^{n} \hat{Z}(X_i)\right)^2}} \tag{18}$$

where $Z(X_i)$ and $\hat{Z}(X_i)$ are the mean of observed and estimated climatic variable values, respectively, and n is the number of paired climatic data.

Then, the model showing the lowest error on the test sample (i.e., the lowest test error) is identified as the best one in this study area. This was the reason why the normality condition was not checked.

3. RESULTS

3.1. Variogram parameter estimation and modeling

For the Mille catchment, in the KED interpolation method with elevation and easting as a covariate, an experimental variogram and two variogram models (i.e., exponential and spherical) automatically fit the theoretical variogram with the experimental variogram. Both monthly and annual variogram parameters, namely range, nugget, and sill, were generated using historic climatic variable data (Table 3).

Dissimilarities expressed by semi-variance were increased following the separation distance (lag) increase and resulted in both sampled climatic data close to each other being more similar; hence, their squared difference was less significant than those that were farther apart. The theoretical variogram model rises to a certain distance and then the model levels off, and the distance at which the model first levels off is termed the range parameter. The semi-variance value that reaches the range parameter is known as the sill. For instance, year long-based mean annual and August mean rainfall were used to simulate the experimental variograms using nine sampled stations, which were then fitted with theoretical variograms using spherical and exponential variogram models, respectively (Figure 4). Accordingly, the exponential and spherical values of the two variogram models provided ranges of approximately 38.8 and 12.9 km, nugget effects of 2,608 and 218 mm^2, and sills of approximately 4,029 and 313 mm^2 for the annual and August months, respectively.

As seen from Table 3, among the two models used, the spherical model was the most frequently applied to fit the monthly experimental semivariogram with the theoretical variogram. For most months (9 out of 12), the theoretical variogram was fitted with an experimental variogram by using the same model, and the same covariates resulted in the same range, but

Table 3 | Variogram parameters and variogram models were developed for the Mille catchment using the KED interpolation technique with the combination of elevation and easting as covariates

Month	Range (m)	Nugget (mm^2)	Sill (mm^2)	Model	Selected covariate/predictor
Jan	12,925	18	22	Spherical	Elevation + easting
Feb	12,925	6	6.8	Spherical	Elevation + easting
Mar	12,925	11	21	Spherical	Elevation + easting
Apr	12,925	19	24	Spherical	Elevation + easting
May	12,925	24	30	Spherical	Elevation + easting
Jun	12,925	10	15	Spherical	Elevation + easting
Jul	38,775	211	888	Exponential	Elevation + easting
Aug	12,925	218	313	Spherical	Elevation + easting
Sep	12,925	26	38	Spherical	Elevation + easting
Oct	38,775	28	43	Exponential	Elevation + easting
Nov	38,775	0.55	0.73	Exponential	Elevation + easting
Dec	12,925	1.6	3.6	Spherical	Elevation + easting
Annual	38,775	2,608	4,029	Exponential	Elevation + easting

the sill and nugget varied, which may be in connection with the spatial pattern and smaller sample size of the sampled rainfall data over the fixed domain (Kaufman & Shaby 2013). Moreover, unlike the spherical model, since the exponential model asymptotically approaches the sill, the effective range was three times the actual range parameter (a) ($a^* = 3a$) (Goovaerts 1997; Nalder & Wein 1998), which means that the proximity by which the spatial dependency decay was longer than the spherical model's effective range (see Table 3).

For the mean minimum and maximum temperatures, both the spherical and exponential variogram models were fitted to the mean annual and monthly (e.g., April month) experimental variograms (Figure 5(a)–5(d)). For the mean minimum annual temperature, the theoretical variogram was fitted to the experimental variogram using an exponential model with a range of 38.8 km, a sill of 0.16°C^2, and a nugget effect of 0.06°C^2. For April, the theoretical variogram was fitted to the experimental variogram using a spherical model with a range of 12.93 km, a sill of 0.2°C^2, and a nugget effect of 0.16°C^2. The same procedure was applied for the mean maximum temperature; as a result, unlike the minimum temperature, both mean monthly (e.g., April) and mean annual maximum temperature experimental variograms were fitted using a spherical model with the same range of 12.93 km but with nugget effects of 0.69 and 0.48°C^2 and sills of approximately 0.83 and 0.9°C^2, respectively.

As depicted in Figure 5(a)–5(d), the number of bins (each possesses 11 and 8 paired climatic datasets) was highly scattered, and these were the results of the sample size and/or the density of sampled climatic data (see Figure 1), which may affect the reliability of the experimental variogram complements to the statistical distribution of the sampled data (Webster & Oliver 2007). According to Webster & Oliver (2007), the reliability of the experimental variogram is affected by factors, namely the size/density of the sampled data (e.g., Ly *et al.* 2011), the statistical distribution of the sampled data, and the configuration or design of the sample. As the sample data size increases, such scatter decreases, and the plotted paired points (bins) tend to be closer to a theoretical variogram (e.g., Figure 6).

In the case of the Akaki catchment, satisfactory computation results were obtained in response to the success in producing an experimental variogram (Table 4 and Figure 6) and have resulted in successful attempts at fitting theoretical variograms with experimental variograms for both mean monthly and annual rainfall and the mean maximum temperature.

For instance, in KED with northing as a covariate, the theoretical variogram was fitted with an experimental variogram model using the spherical model with a range of 4.9 km, a sill of 0.65 mm^2, and a nugget effect of 0.3 mm^2 for January mean monthly rainfall, and the Ste model was fitted to the theoretical variogram and the experimental variogram using a range of 7.5 km, a sill variance of 1,943 mm^2, and a nugget variance of 0 mm^2 for the mean annual rainfall.

Overall, the variogram value is often zero at a lag distance equal to zero in theory. Nevertheless, within the shortest distance, which is less than lag, the variogram often exhibits the phenomenon called the 'nugget effect', which is a value

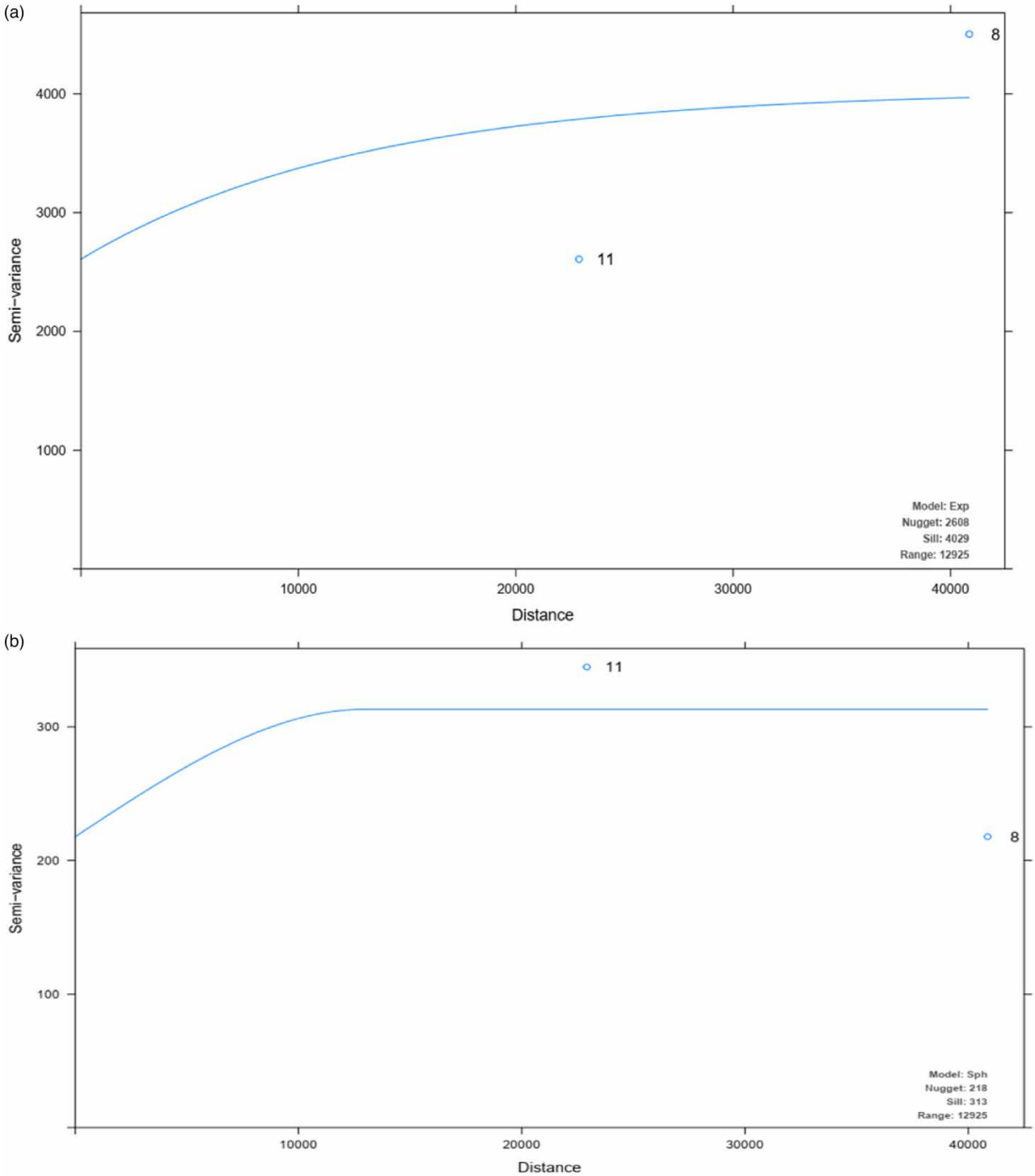

Figure 4 | Empirical and theoretical semivariogram models: exponential (a) and spherical (b) for annual and August monthly mean rainfall, respectively.

greater than zero (Webster & Oliver 2007). The nugget effect can be attributed to measurement errors, which occur because of the error inherent in measuring devices, or spatial sources of variation at microscale distances smaller than the lag distance (or both).

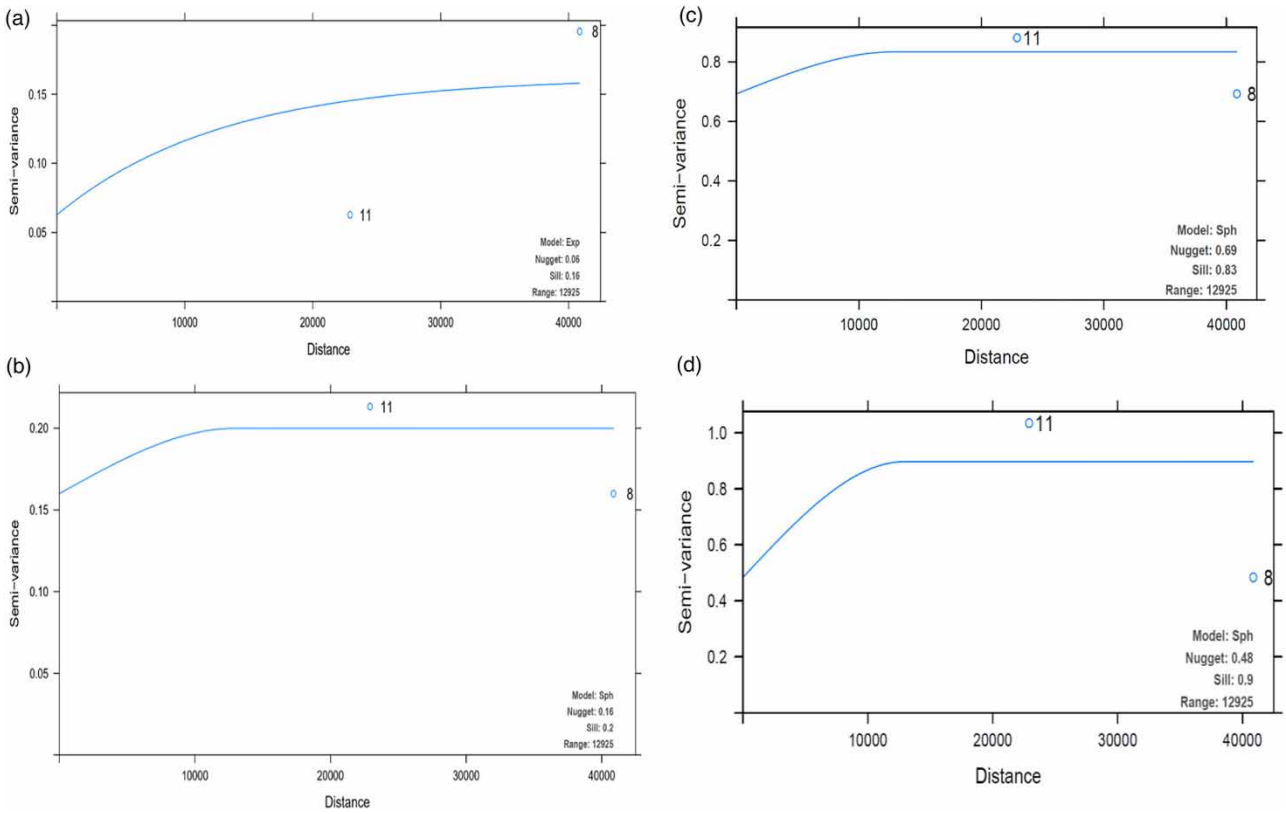

Figure 5 | Empirical and theoretical semivariogram models: exponential (a) and spherical (b) for annual and April mean minimum temperatures and spherical (c and d) for annual and April mean maximum temperatures.

3.2. Verifying the performance of interpolation methods via the LOOCV procedure

All the methods described in subsection 2.3.2. were performed and evaluated through a cross-validation technique, specifically the LOOCV method, which allows us to compare estimated and actual values using sampled data (Isaaks 1990) (e.g., Mille catchment rainfall and maximum temperature; Tables 5 and 6). The results in Table 5 show that the KED using the combination of longitude and elevation gives overall the best spatial estimation results with the smallest statistical evaluation parameters, followed by KED with longitude alone as a covariate and IDW and KED with elevation as the covariates.

For example, in the case of the August month rainfall, some interpolation techniques with and without predictors, for example, KED using northing as a predictor and OK, both show relatively higher statistical indicators than the rest of the interpolation methods. In contrast, IDW shows higher performance with the lowest statistical indicators than KED with elevation/northing as the covariate.

The combination of predictors, for instance easting and elevation used by KED, significantly improves the prediction of sampled mean monthly and annual rainfall data. Therefore, KED with the combination of two predictors, elevation and easting (Table 5), seems to be the optimum method to predict mean monthly climatic data (e.g., August: RMSE = 20.66, $r = 0.96$, and mean annual rainfall: RMSE = 75.62, MBE = 3.61, $r = 0.96$). However, the KED with predictors, i.e. northing and OK, shows the worst results (RMSE = 258.35, MAE = 204.18, and RMSE = 245.72, MAE = 192.64), respectively.

Accordingly, based on the statistical evaluation results, KED with the combination of elevation and easting as a covariate was selected as the optimum spatial interpolation technique for Mille's catchment area mean rainfall estimation.

Similarly, Table 6 illustrates the performance of the different prediction methods for estimating the monthly and annual maximum temperatures for the Mille catchment in terms of statistical indicators, namely RMSE, MBE, MAE, and r. The smaller the values of statistical parameters (and the higher the r-value), the better the predictor/s with the corresponding interpolation techniques (Adhikary *et al.* 2017). As a result, Table 6 presents the performance of the various prediction techniques for the mean

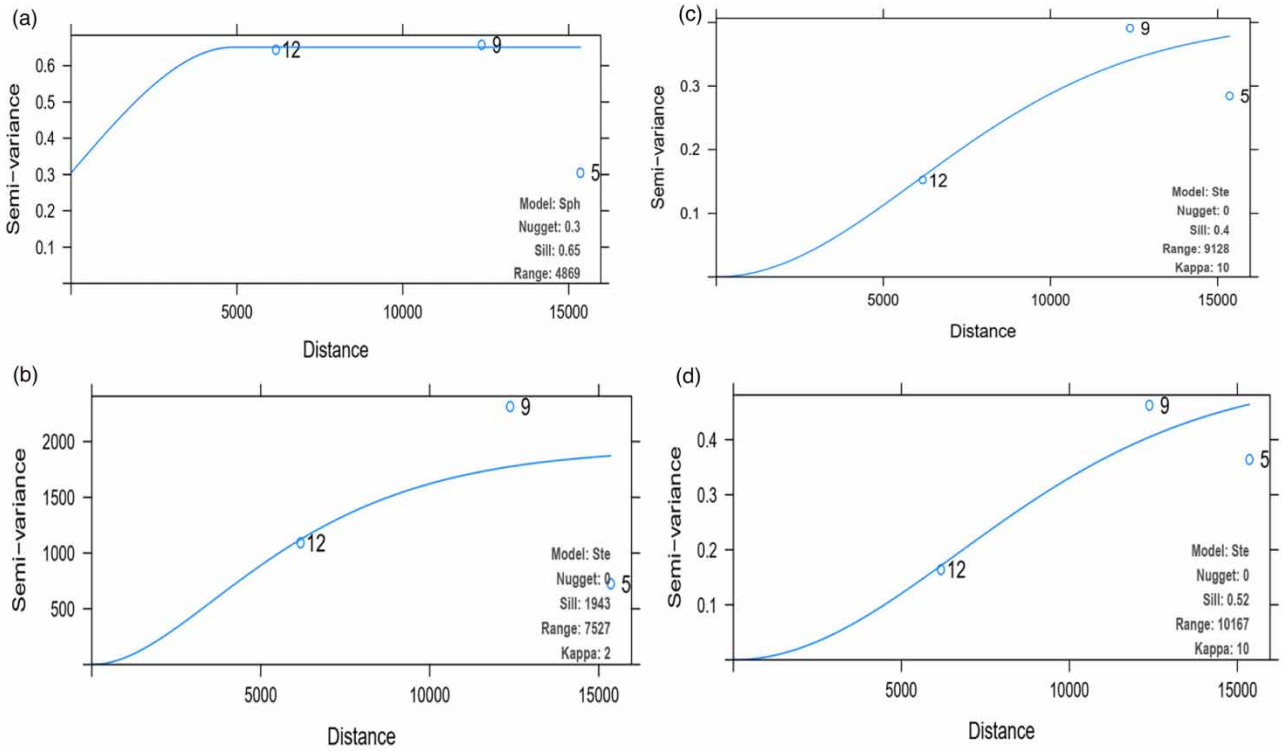

Figure 6 | Experimental (bins) and fitted theoretical (curve) variograms of January mean monthly ((a) and (c)) and annual ((b) and (d)) rainfall and maximum temperature, respectively.

Table 4 | Variogram parameters and models developed for Akaki's catchment mean monthly and annual rainfall and maximum temperature using KED with various covariates

Parameters and variogram model for mean rainfall						Parameters and variogram model for mean T_{max}				
Month	**Range**	**Nugget**	**Sill**	**Model**	**Covariates**	**Range**	**Nugget**	**Sill**	**Model**	**Covariates**
Jan	4,869	0.3	0.65	Spherical	Northing	9,128	0	0.4	Ste	Elevation + northing
Feb	12,471	0	12	Ste	Easting	8,915	0	0.45	Ste	Elevation + northing
Mar	8,295	0	24	Ste	Easting	9,224	0	0.5	Ste	Elevation + northing
Apr	5,725	0	14	Ste	Northing	9,954	0	0.56	Ste	Elevation
May	11,838	0	24	Ste	Easting	10,962	0	0.72	Ste	Elevation
Jun	4,743	0	17	Ste	Elevation	9,057	0	0.62	Ste	Elevation
Jul	6,015	0	231	Ste	Northing	9,666	0	0.71	Ste	Elevation
Aug	8,954	0	504	Ste	Northing	9,447	0	0.58	Ste	Elevation
Sep	5,240	0	106	Ste	Elevation	10,489	0	0.51	Ste	Elevation
Oct	2,904	0	10	Ste	Easting	8,931	0	0.6	Ste	Elevation + northing
Nov	9,547	0	2.2	Ste	Elevation	8,526	0	0.43	Ste	Elevation + northing
Dec	9,773	0	1.5	Ste	Easting	8,384	0	0.42	Ste	Elevation + northing
Annual	7,527	0	1,943	Ste	Northing	10,658	0	2,496	Ste	Elevation

annual and monthly maximum temperatures for 12 months. Based on the estimated results, there was little difference between KED with the combination of elevation and easting as a covariate and KED with elevation alone as a covariate followed by IDW, and these interpolation techniques performed better than the rest of the methods for spatial prediction and mean monthly

Table 5 | Mille catchment's mean monthly and annual rainfall spatial prediction using various interpolation techniques

Month	Est. rainfall[a]	Obr. rainfall[a]	RMSE	MBE	MAE	r	V.model	Month	Est. rainfall	Obr. rainfall	RMSE	MBE	MAE	r	V.model
KED with 90 m DEM elevation								**KED with the combination of 90 m DEM elevation and easting**							
Jan	11.79	11.42	5.71	−0.36	5.05	−0.01	Spherical	Jan	11.62	11.42	5.41	−0.20	4.56	0.30	Spherical
Feb	6.75	6.80	3.17	0.05	2.62	0.57	Spherical	Feb	6.42	6.80	3.89	0.38	3.21	0.5	Spherical
Mar	38.33	37.92	9.07	−0.42	8.09	0.86	Exponential	Mar	37.17	37.92	7.31	0.75	6.38	0.92	Spherical
Apr	58.14	57.64	9.92	−0.50	8.37	0.86	Exponential	Apr	57.04	57.64	7.69	0.6	6.49	0.93	Spherical
May	43.95	43.40	9.27	−0.56	8.46	0.84	Exponential	May	43.18	43.40	6.68	0.22	5.61	0.92	Spherical
Jun	16.62	16.49	4.36	−0.13	3.61	0.88	Exponential	Jun	16.59	16.49	4.41	−0.1	3.34	0.88	Spherical
Jul	194.87	192.76	36.00	−2.12	30.40	0.89	Exponential	Jul	193.10	192.76	26.85	−0.36	19.22	0.94	Exponential
Aug	218.10	216.06	34.90	−2.05	32.46	0.88	Exponential	Aug	214.80	216.06	20.66	1.26	18.5	0.96	Spherical
Sep	64.69	64.03	13.45	−0.67	11.27	0.87	Exponential	Sep	63.46	64.03	9.3	0.56	7.6	0.95	Spherical
Oct	24.64	24.16	7.39	−0.48	6.35	0.75	Exponential	Oct	24.45	24.16	7.07	−0.3	6.21	0.77	Exponential
Nov	16.25	16.08	2.77	−0.17	2.50	0.85	Exponential	Nov	16.01	16.08	1.28	0.07	1.04	0.97	Exponential
Dec	12.23	12.00	4.71	−0.24	3.88	0.50	Exponential	Dec	11.72	12.00	2.82	0.28	2.41	0.88	Spherical
Annual	706.40	698.80	124.17	−7.67	110.66	0.88	Exponential	Annual	695.1	698.8	75.32	3.70	67.99	0.96	Exponential
KED with easting alone as a covariate								**IDW**							
Jan	11.81	11.42	4.90	−0.39	4.42	0.40	Exponential	Jan	10.88	11.42	3.86	0.54	2.55	0.69	–
Feb	6.35	6.80	3.63	0.45	2.90	0.52	Spherical	Feb	7.30	6.80	2.92	−0.50	2.66	0.67	–
Mar	37.25	37.92	7.10	0.66	5.71	0.93	Spherical	Mar	40.09	37.92	6.96	−2.17	6.23	0.93	–
Apr	57.24	57.64	7.66	0.40	6.06	0.93	Spherical	Apr	59.50	57.64	6.87	−1.86	5.23	0.94	–
May	43.47	43.40	6.42	−0.07	5.18	0.93	Spherical	May	45.02	43.40	6.16	−1.62	5.78	0.94	–
Jun	16.43	16.49	5.47	0.06	4.58	0.81	Spherical	Jun	17.86	16.49	3.81	−1.37	3.33	0.92	–
Jul	193.78	192.76	25.38	−1.02	19.88	0.95	Exponential	Jul	204.34	192.76	29.32	−11.58	26.31	0.94	–
Aug	215.25	216.06	22.27	0.82	18.45	0.95	Spherical	Aug	227.10	216.06	23.15	−11.04	18.97	0.96	–
Sep	63.44	64.03	8.92	0.58	7.14	0.95	Spherical	Sep	66.31	64.03	9.67	−2.28	8.21	0.94	–
Oct	24.76	24.16	6.37	−0.60	5.46	0.82	Exponential	Oct	24.98	24.16	3.40	−0.83	2.72	0.97	–
Nov	16.02	16.08	1.12	0.06	0.90	0.98	Exponential	Nov	16.65	16.08	1.12	−0.56	0.92	0.99	–
Dec	11.87	12.00	2.81	0.12	2.31	0.86	Exponential	Dec	11.91	12.00	2.68	0.08	2.52	0.87	–
Annual	697.40	698.80	78.39	1.37	66.75	0.96	Exponential	Annual	731.90	698.80	77.34	−33.18	69.51	0.97	–
KED with northing alone as a covariate								**OK**							
Jan	11.45	11.42	5.95	−0.02	4.62	−0.15	Spherical	Jan	11.45	11.42	5.85	−0.03	4.77	−0.99	Exponential
Feb	6.54	6.80	4.65	0.26	4.11	−0.75	Exponential	Feb	6.85	6.80	3.93	−0.05	3.55	−0.59	Exponential
Mar	37.98	37.92	18.01	−0.06	15.36	−0.10	Exponential	Mar	38.73	37.92	16.71	−0.81	13.29	0.40	Exponential

(*Continued.*)

Table 5 | Continued

Month	Est. rainfall[a]	Obr. rainfall[a]	RMSE	MBE	MAE	*r*	V.model	Month	Est. rainfall	Obr. rainfall	RMSE	MBE	MAE	*r*	V.model
Apr	58.06	57.64	19.88	−0.42	16.58	−0.02	Exponential	Apr	58.67	57.64	18.67	−1.03	14.90	0.40	Exponential
May	43.07	43.40	18.51	0.33	15.13	−0.56	Exponential	May	44.00	43.40	17.01	−0.60	13.78	−0.01	Exponential
Jun	16.19	16.49	10.18	0.30	8.16	−0.26	Exponential	Jun	16.71	16.49	9.25	−0.22	7.38	−0.24	Exponential
Jul	197.60	192.76	75.24	−4.79	56.99	0.41	Exponential	Jul	198.00	192.76	71.71	−5.25	54.10	0.60	Exponential
Aug	217.50	216.06	72.55	−1.47	57.69	0.03	Exponential	Aug	267.50	269.30	68.54	−3.67	52.78	0.48	Exponential
Sep	64.55	64.03	27.91	−0.52	23.91	−0.03	Exponential	Sep	65.26	64.03	26.61	−1.23	21.37	0.29	Exponential
Oct	24.23	24.16	11.88	−0.07	9.26	−0.73	Exponential	Oct	24.53	24.16	11.26	−0.37	8.70	−0.15	Exponential
Nov	16.38	16.08	4.87	−0.29	4.18	0.38	Exponential	Nov	16.44	16.08	4.77	−0.35	3.62	0.63	Exponential
Dec	11.82	12.00	5.02	0.18	4.20	0.43	Exponential	Dec	12.13	12.00	5.57	−0.14	4.71	−0.25	Exponential
Annual	708.80	698.80	258.35	−10.04	204.18	0.25	Exponential	Annual	714.40	698.80	245.72	−15.61	192.64	0.53	Exponential

[a]Est. rainfall, estimated rainfall; Obr. rainfall, observed rainfall.

Table 6 | Mille catchment's mean monthly and annual maximum temperature estimated and actual values, and descriptive statistics using various interpolation techniques

Month	Est. T^a_{max}	Obr. T^a_{max}	RMSE	MBE	MAE	r	V.model	Month	Est. T_{max}	Obr. T_{max}	RMSE	MBE	MAE	r	V.model
KED with 90 m DEM elevation								**KED with the combination of 90 m DEM elevation and easting as a covariate**							
Jan	31.71	31.62	1.72	−0.09	1.41	0.90	Exponential	Jan	31.62	31.62	1.401	0.006	1.29	0.93	Exponential
Feb	33.45	33.47	0.67	0.02	0.61	0.98	Spherical	Feb	33.45	33.47	0.706	0.024	0.625	0.9824	Spherical
Mar	36.11	36.06	1.68	−0.05	1.50	0.94	Spherical	Mar	35.92	36.06	1.734	0.143	1.542	0.9345	Spherical
Apr	36.77	36.69	1.44	−0.08	1.13	0.97	Spherical	Apr	36.77	36.69	1.269	−0.082	1.116	0.9752	Spherical
May	37.38	37.36	0.90	−0.02	0.80	0.99	Spherical	May	37.38	37.36	0.972	−0.014	0.859	0.9828	Spherical
Jun	39.08	39.01	1.88	−0.07	1.72	0.94	Exponential	Jun	39.07	39.01	1.860	−0.056	1.738	0.9426	Exponential
Jul	38.99	38.86	2.20	−0.14	1.86	0.93	Exponential	Jul	38.92	38.86	2.066	−0.059	1.763	0.9404	Exponential
Aug	35.85	35.77	1.42	−0.08	1.13	0.97	Spherical	Aug	35.89	35.77	1.452	−0.115	1.174	0.9747	Spherical
Sep	34.32	34.38	1.64	0.06	1.24	0.96	Exponential	Sep	34.55	34.38	1.779	−0.177	1.498	0.956	Exponential
Oct	34.36	34.33	1.15	−0.03	0.99	0.98	Spherical	Oct	34.43	34.33	1.348	−0.100	1.2	0.97	Spherical
Nov	33.18	33.04	2.14	−0.14	1.82	0.92	Exponential	Nov	33.06	33.04	1.762	−0.022	1.43	0.94	Spherical
Dec	30.43	30.42	0.62	−0.02	0.52	0.99	Spherical	Dec	30.44	30.42	0.595	−0.021	0.531	0.99	Spherical
Annual	35.13	35.08	1.16	−0.05	1.03	0.97	Spherical	Annual	35.11	35.08	1.150	−0.029	1.06	0.97	Spherical
KED with easting alone as a covariate								**IDW**							
Jan	31.84	31.62	2.92	−0.22	2.41	0.68	Exponential	Jan	31.17	31.62	1.54	0.46	1.37	0.94	–
Feb	33.55	33.47	1.76	−0.08	1.48	0.89	Exponential	Feb	32.98	33.47	1.47	0.49	1.26	0.94	–
Mar	36.25	36.06	3.18	−0.19	2.74	0.77	Exponential	Mar	35.44	36.06	2.49	0.62	2.09	0.87	–
Apr	36.99	36.69	3.76	−0.30	3.31	0.77	Exponential	Apr	35.96	36.69	2.12	0.73	1.76	0.94	–
May	37.56	37.36	2.83	−0.20	2.37	0.85	Exponential	May	36.64	37.36	1.70	0.72	1.39	0.96	–
Jun	39.34	39.01	3.78	−0.33	2.98	0.76	Exponential	Jun	38.36	39.01	1.83	0.66	1.55	0.96	–
Jul	39.18	38.86	4.04	−0.32	3.36	0.76	Exponential	Jul	38.04	38.86	2.07	0.82	1.67	0.96	–
Aug	36.10	35.77	3.98	−0.33	3.55	0.80	Exponential	Aug	34.91	35.77	2.44	0.86	1.86	0.93	–
Sep	34.54	34.38	2.74	−0.16	2.37	0.89	Exponential	Sep	33.59	34.38	2.47	0.78	1.98	0.92	–
Oct	34.61	34.33	3.24	−0.27	2.82	0.83	Exponential	Oct	33.61	34.33	2.04	0.72	1.65	0.94	–
Nov	33.32	33.04	3.82	−0.28	3.41	0.71	Exponential	Nov	32.36	33.04	2.65	0.68	2.02	0.87	–
Dec	30.57	30.42	2.30	−0.15	2.00	0.82	Exponential	Dec	29.85	30.42	1.20	0.56	1.08	0.97	–
Annual	35.32	35.08	3.09	−0.24	2.66	0.81	Exponential	Annual	34.41	35.08	1.86	0.68	1.57	0.94	–
KED with northing alone as a covariate								**OK**							
Jan	31.59	31.62	3.93	0.04	3.82	0.11	Exponential	Jan	31.47	31.62	3.55	0.16	3.40	0.61	Exponential
Feb	33.38	33.47	3.77	0.10	3.54	0.10	Exponential	Feb	33.29	33.47	3.50	0.18	3.21	0.60	Exponential
Mar	35.91	36.06	4.89	0.15	4.64	0.11	Exponential	Mar	35.84	36.06	4.47	0.22	4.14	0.55	Exponential

(*Continued.*)

Table 6 | Continued

Month	Est. T^a_{max}	Obr. T^a_{max}	RMSE	MBE	MAE	*r*	V.model	Month	Est. T_{max}	Obr. T_{max}	RMSE	MBE	MAE	*r*	V.model
Apr	36.50	36.69	5.46	0.18	5.26	0.21	Exponential	Apr	36.40	36.69	4.97	0.29	4.74	0.72	Exponential
May	37.21	37.36	5.07	0.16	4.90	0.24	Exponential	May	37.09	37.36	4.63	0.28	4.43	0.74	Exponential
Jun	38.89	39.01	5.60	0.12	5.46	0.07	Exponential	Jun	38.76	39.01	5.00	0.25	4.88	0.67	Exponential
Jul	38.70	38.86	5.91	0.15	5.74	0.23	Exponential	Jul	38.55	38.86	5.28	0.31	5.13	0.77	Exponential
Aug	35.51	35.77	6.02	0.26	5.77	0.27	Exponential	Aug	35.43	35.77	5.49	0.35	5.21	0.75	Exponential
Sep	34.10	34.38	5.62	0.28	4.89	0.42	Exponential	Sep	34.04	34.38	5.32	0.33	4.55	0.64	Exponential
Oct	34.14	34.33	5.48	0.19	5.28	0.20	Exponential	Oct	34.04	34.33	5.01	0.29	4.77	0.71	Exponential
Nov	32.94	33.04	5.16	0.10	5.00	0.22	Exponential	Nov	32.79	33.04	4.74	0.25	4.43	0.66	Exponential
Dec	30.26	30.42	3.79	0.16	3.59	0.25	Exponential	Dec	30.20	30.42	3.45	0.22	3.27	0.75	Exponential
Annual	34.92	35.08	4.96	0.16	4.82	0.21	Exponential	Annual	29.85	30.42	1.20	0.56	1.08	0.97	Exponential

and mean annual maximum temperature estimation. Nevertheless, KED with the combination of easting and elevation (see Table 6) seems to be the optimum technique to estimate the mean monthly (e.g., April: RMSE = 1.27, $r = 0.98$) and mean annual maximum temperature (RMSE = 1.15, $r = 0.97$). Therefore, it was selected for monthly and annual mean maximum temperature spatial prediction as an optimum interpolation technique. For the maximum temperature and mean rainfall, KED with easting and elevation as covariates seems to be the most suitable technique to predict the mean minimum temperature, since, for most months, the statistical parameters were the lowest with the aforementioned method.

Figures 7 and 8 are a map of different interpolation techniques with and without covariates for August rainfall and the mean annual maximum temperature of the Mille catchment to visualize the spatial pattern of predicted mean rainfall and mean maximum temperature, and the maps show the fundamental differences between the various interpolation approaches.

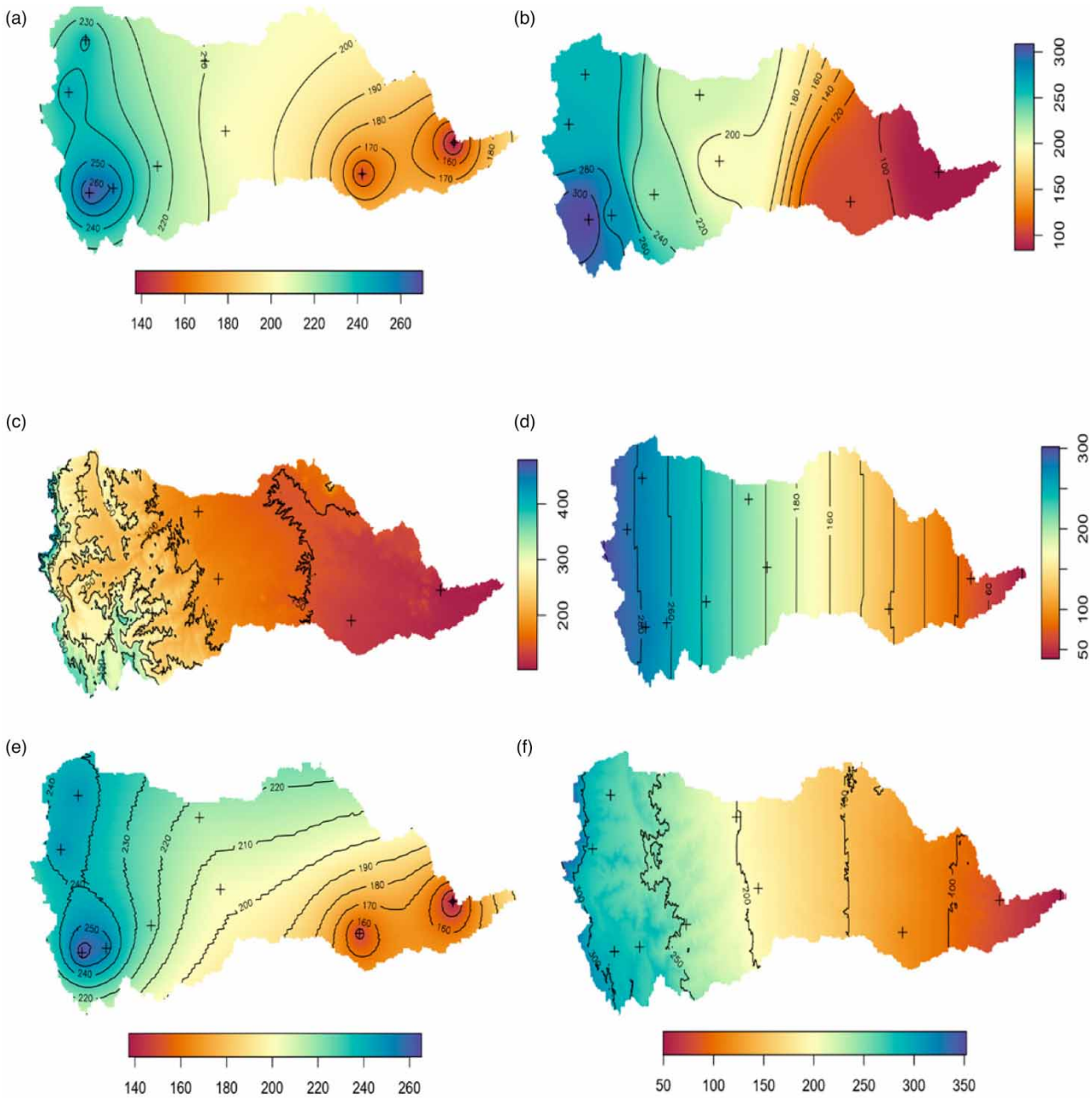

Figure 7 | Spatial maps for the August mean rainfall (mm) pattern using OK (a), IDW (b), KED with elevation (c), KED with easting (d), KED with northing (e), and KED with the combination of elevation and easting (f) by the interpolation of nine sampled observations.

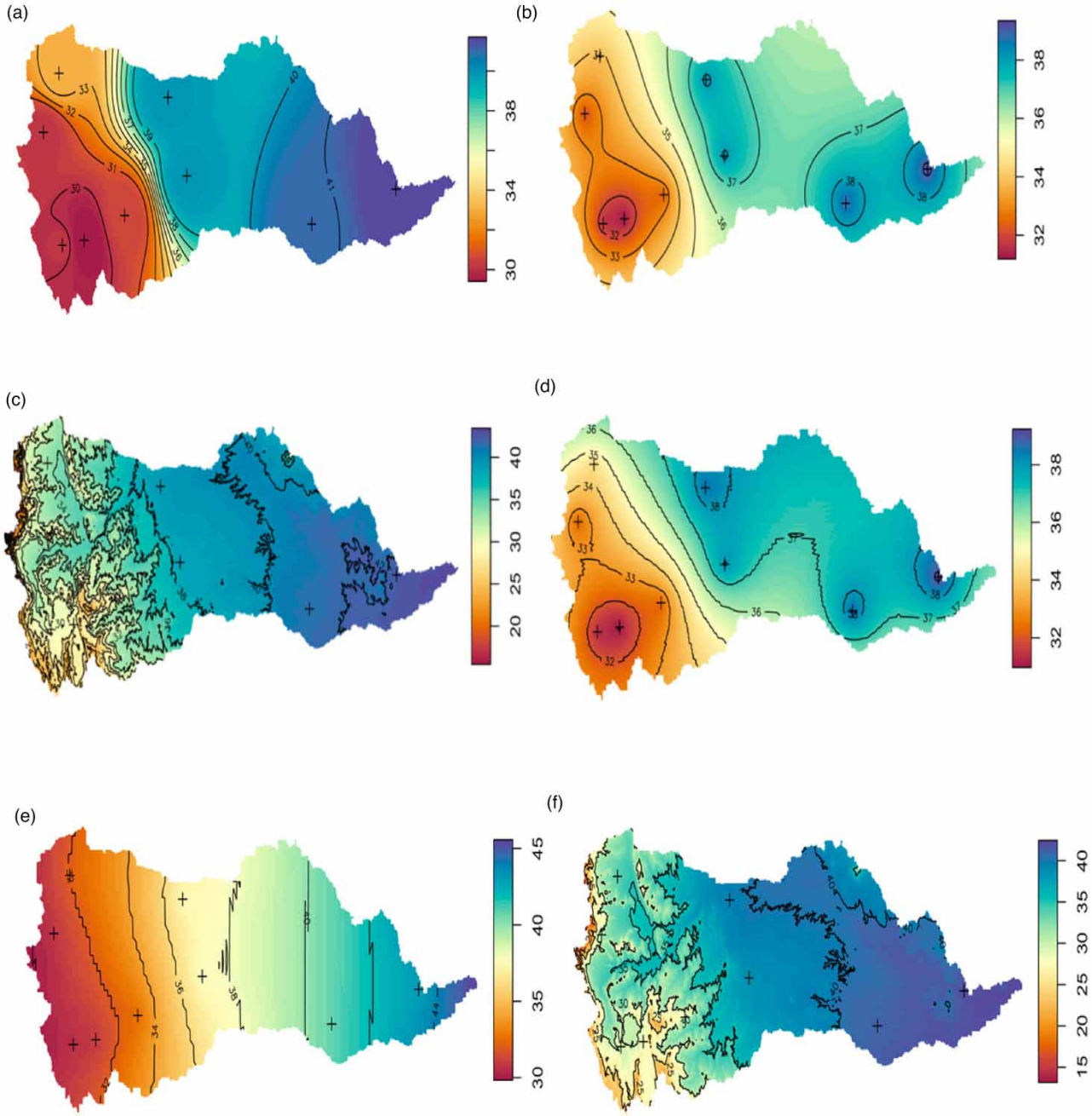

Figure 8 | Spatial maps for the annual mean maximum temperature (°C) pattern using IDW (a), OK (b), KED with elevation (c), KED with northing (d), KED with easting (e), and KED with the combination of elevation and easting (f) by the interpolation of nine sampled observations.

For the Akaki catchment, Tables 7 and 8 present the performance of different interpolation methods for predicting both mean monthly and mean annual climatic variables. These interpolation techniques were quantitatively compared based on evaluation performance scores to identify a suitable method for the spatial prediction of climatic variables at the catchment scale. As depicted in Table 7, overall, KED with northing as a covariate and KED with easting as a covariate perform relatively better than the rest of the interpolation techniques, specifically OK, IDW, and KED, with elevation as a covariate for mean monthly rainfall estimation. For mean annual rainfall, KED with elevation as a covariate performs better than the rest of the interpolation methods (e.g., RMSE = 40.28 mm, MBE = −10.43 mm, and MAE = 33.54 mm). Nevertheless, KED with

Table 7 | Akaki catchment long year-based predicted vs. observed mean monthly and annual rainfall using various interpolation techniques

Month	Est. rainfall	Obr. rainfall	RMSE	MBE	MAE	r	V.model	Month	Est. rainfall	Obr. rainfall	RMSE	MBE	MAE	r	V.model
KED with 90 m DEM elevation								**IDW**							
Jan	6.650	6.652	0.99	0.002	0.81	0.59	Exponential	Jan	6.85	6.65	1.17	−0.19	0.94	0.31	–
Feb	9.58	9.14	2.48	−0.44	1.93	0.46	Exponential	Feb	9.94	9.14	2.05	−0.80	1.60	0.66	–
Mar	34.73	34.14	2.95	−0.59	2.78	0.54	Ste	Mar	35.65	34.14	4.07	−1.51	2.94	0.54	–
Apr	55.09	55.78	3.92	0.69	1.94	0.47	Ste	Apr	55.35	55.78	2.41	0.43	1.90	0.67	–
May	66.20	64.89	6.99	−1.31	4.68	0.31	Ste	May	67.89	64.89	7.60	−3.00	4.61	0.22	–
Jun	114.60	113.50	4.47	−1.08	3.74	0.80	Ste	Jun	115.40	113.50	5.72	−1.93	4.75	0.65	–
Jul	249.10	248.60	17.49	−0.49	11.84	0.52	Ste	Jul	248.30	248.60	17.55	0.35	14.22	0.36	–
Aug	267.00	265.40	23.48	−1.57	16.48	0.46	Ste	Aug	267.80	265.40	25.60	−2.39	20.26	0.23	–
Sep	128.50	123.90	10.51	−4.56	8.27	0.74	Ste	Sep	130.40	123.90	11.51	−6.45	9.83	0.75	–
Oct	16.77	15.86	4.01	−0.91	2.73	0.50	Ste	Oct	17.96	15.86	4.32	−2.10	3.17	0.62	–
Nov	6.60	6.08	1.16	−0.52	0.78	0.69	Ste	Nov	6.74	6.08	1.24	−0.66	0.98	0.77	–
Dec	5.73	5.69	1.26	−0.05	1.05	0.15	Ste	Dec	5.96	5.69	1.14	−0.27	0.84	0.34	–
Annual	960.10	949.70	40.28	−10.43	33.54	0.65	Ste	Annual	968.20	949.70	48.20	−18.53	41.72	0.50	–
KED with easting alone as a covariate								**OK**							
Jan	6.84	6.65	1.48	−0.19	1.01	−0.42	Exponential	Jan	6.70	6.65	1.29	−0.05	0.95	−0.315	Exponential
Feb	9.48	9.14	1.70	−0.34	1.45	0.76	Ste	Feb	9.78	9.14	2.16	−0.64	1.67	0.606	Ste
Mar	33.95	34.14	2.28	0.19	1.88	0.86	Ste	Mar	34.75	34.14	3.82	−0.61	2.67	0.544	Ste
Apr	55.96	55.78	3.10	−0.18	2.13	0.53	Ste	Apr	55.18	55.78	2.38	0.60	1.58	0.687	Ste
May	64.84	64.89	5.18	0.05	3.32	0.69	Ste	May	66.29	64.89	7.00	−1.40	4.66	0.312	Ste
Jun	113.50	113.50	5.98	−0.05	5.00	0.56	Exponential	Jun	113.80	113.50	6.41	−0.30	5.50	0.518	Exponential
Jul	244.40	248.60	25.23	4.27	19.11	−0.59	Ste	Jul	248.40	248.60	20.16	0.22	16.23	−0.702	Exponential
Aug	259.90	265.40	49.75	5.49	30.66	−0.56	Ste	Aug	266.30	265.40	28.40	−0.91	22.06	−0.509	Exponential
Sep	121.81	123.90	12.24	2.10	8.79	0.75	Exponential	Sep	127.70	123.90	8.41	−3.80	6.51	0.865	Ste
Oct	15.81	15.86	1.85	0.06	1.56	0.92	Ste	Oct	15.87	15.86	4.99	−0.01	4.08	−0.997	Ste
Nov	5.98	6.08	1.58	0.10	1.07	0.61	Ste	Nov	6.58	6.08	1.05	−0.50	0.87	0.85	Ste
Dec	5.70	5.69	0.96	−0.01	0.71	0.58	Ste	Dec	5.77	5.69	0.95	−0.08	0.65	0.60	Ste
Annual	940.50	949.70	91.14	9.13	61.53	0.07	Ste	Annual	952.80	949.70	51.53	−3.181	42.24	0.07	Exponential
KED with northing alone as a covariate								**KED with the combination 90 m DEM elevation and northing as a covariate**							
Jan	6.71	6.65	0.73	−0.05	0.59	0.79	Spherical	Jan	6.85	6.65	1.07	−0.20	0.83	0.52	Ste
Feb	10.17	9.14	4.59	−1.03	2.79	−0.01	Ste	Feb	10.17	9.14	3.43	−1.04	2.33	0.08	Ste
Mar	35.38	34.14	4.88	−1.24	3.12	0.24	Ste	Mar	36.46	34.14	8.22	−2.32	4.66	−0.34	Ste

(*Continued.*)

Table 7 | Continued

Month	Est. rainfall	Obr. rainfall	RMSE	MBE	MAE	*r*	V.model	Month	Est. rainfall	Obr. rainfall	RMSE	MBE	MAE	*r*	V.model
Apr	55.31	55.78	2.36	0.48	1.63	0.69	Ste	Apr	55.51	55.78	3.68	0.27	2.38	0.35	Ste
May	67.79	64.89	10.16	−2.90	6.23	−0.53	Ste	May	69.39	64.89	13.82	−4.50	8.02	−0.82	Ste
Jun	114.40	113.50	8.22	−0.93	6.19	0.15	Exponential	Jun	114.70	113.50	3.69	−1.23	3.19	0.88	Ste
Jul	249.10	248.60	14.14	−0.46	12.37	0.69	Ste	Jul	246.70	248.60	23.78	1.98	17.88	0.18	Ste
Aug	268.60	265.40	11.35	−3.25	8.88	0.92	Ste	Aug	268.10	265.40	20.61	−2.69	15.95	0.62	Ste
Sep	129.70	123.90	5.16	−5.81	8.77	0.55	Ste	Sep	131.90	123.90	16.51	−7.97	11.28	0.20	Ste
Oct	17.55	15.86	5.16	−1.69	3.14	0.17	Ste	Oct	18.73	15.86	8.31	−2.87	4.47	−0.47	Ste
Nov	6.82	6.08	1.44	−0.73	1.10	0.50	Ste	Nov	6.61	6.08	1.37	−0.53	0.84	0.51	Ste
Dec	5.95	5.69	1.40	−0.26	1.07	0.08	Ste	Dec	6.17	5.69	2.20	−0.48	1.54	−0.13	Ste
Annual	967.10	949.70	41.78	−17.41	35.59	0.67	Ste	Annual	969.80	949.70	47.72	−20.10	40.51	0.57	Ste

Table 8 | Akaki catchment long year-based predicted vs. observed mean monthly and annual maximum temperature using various interpolation techniques

Month	Est. T_{max}	Obr. T_{max}	RMSE	MBE	MAE	r	V.model	Month	Est. T_{max}	Obr. T_{max}	RMSE	MBE	MAE	r	V.model
KED with 90 m DEM elevation								**IDW**							
Jan	23.56	23.68	0.83	0.1250	0.69	0.80	Ste	Jan	23.56	23.68	1.04	0.126	0.89	0.68	–
Feb	24.83	24.96	0.83	0.13	0.69	0.81	Ste	Feb	24.82	24.96	1.08	0.14	0.92	0.68	–
Mar	25.03	25.17	0.94	0.1415	0.77	0.76	Ste	Mar	25.03	25.17	1.09	0.1453	0.93	0.67	–
Apr	24.53	24.70	0.95	0.16	0.76	0.75	Ste	Apr	24.49	24.70	1.15	0.20	0.95	0.64	–
May	24.56	24.77	1.10	0.22	0.84	0.70	Ste	May	24.50	24.77	1.20	0.27	0.95	0.65	–
Jun	22.91	23.17	0.89	0.26	0.67	0.82	Ste	Jun	22.79	23.17	1.23	0.38	0.98	0.67	–
Jul	20.75	20.99	0.89	0.233	0.67	0.80	Ste	Jul	20.66	20.99	1.21	0.32	0.98	0.63	–
Aug	20.30	20.51	0.79	0.21	0.61	0.83	Ste	Aug	20.23	20.51	1.12	0.28	0.92	0.66	–
Sep	21.49	21.69	0.84	0.19	0.63	0.83	Ste	Sep	21.46	21.69	1.13	0.22	0.89	0.70	–
Oct	22.74	22.89	0.93	0.15	0.78	0.80	Ste	Oct	22.74	22.89	1.16	0.15	1.00	0.67	–
Nov	23.02	23.15	0.86	0.13	0.71	0.81	Ste	Nov	23.05	23.15	1.06	0.10	0.10	0.69	–
Dec	22.77	22.86	0.78	0.10	0.64	0.79	Ste	Dec	22.77	22.86	0.99	0.10	0.86	0.67	–
Annual	23.03	23.20	0.87	0.17	0.69	0.80	Ste	Annual	22.75	22.81	0.92	0.06	0.73	0.67	–
KED with easting as a covariate								**OK**							
Jan	23.84	23.68	1.56	−0.15	1.29	−0.25	Exponential	Jan	23.677	23.684	1.31	0.01	1.11	0.120	Exponential
Feb	25.13	24.96	1.62	−0.17	1.34	−0.26	Exponential	Feb	24.96	24.97	1.36	0.01	1.14	0.101	Exponential
Mar	25.35	25.17	1.66	−0.18	1.36	−0.29	Exponential	Mar	25.16	25.17	1.37	0.01	1.15	0.044	Exponential
Apr	24.89	24.70	1.73	−0.19	1.41	−0.25	Exponential	Apr	24.68	24.70	1.41	0.02	1.16	−0.035	Exponential
May	24.98	24.77	1.83	−0.21	1.46	−0.15	Exponential	May	24.74	24.77	1.47	0.03	1.17	−0.062	Exponential
Jun	23.34	23.17	1.71	−0.17	1.38	0.08	Exponential	Jun	23.12	23.17	1.46	0.05	1.09	0.094	Exponential
Jul	21.16	20.99	1.70	−0.17	1.40	−0.004	Exponential	Jul	20.95	20.99	1.45	0.04	1.12	−0.052	Exponential
Aug	20.64	20.51	1.54	−0.13	1.30	0.004	Exponential	Aug	20.47	20.51	1.37	0.04	1.08	−0.0002	Exponential
Sep	21.81	21.69	1.60	−0.12	1.34	−0.06	Exponential	Sep	21.66	21.69	1.42	0.03	1.14	0.112	Exponential
Oct	23.08	22.89	1.77	−0.19	1.47	−0.28	Exponential	Oct	22.88	22.89	1.47	0.01	1.25	0.051	Exponential
Nov	23.33	23.15	1.64	−0.17	1.34	−0.29	Spherical	Nov	23.15	23.15	1.36	0.001	1.14	0.14	Exponential
Dec	23.04	22.86	1.54	−0.18	1.25	−0.35	Exponential	Dec	22.86	22.86	1.25	0.001	1.06	0.05	Exponential
Annual	23.37	23.20	1.65	−0.17	1.36	−0.18	Exponential	Annual	23.18	23.20	1.38	0.022	1.13	0.05	Exponential
KED with northing as a covariate								**KED with the combination of northing and 90 m DEM elevation as a covariate**							
Jan	23.60	23.68	0.95	0.08	0.88	0.71	Exponential	Jan	23.37	23.68	0.85	0.32	0.61	0.86	Ste
Feb	24.88	24.96	1.01	0.08	0.94	0.69	Exponential	Feb	24.63	24.96	0.88	0.34	0.64	0.85	Ste
Mar	25.07	25.17	0.99	0.10	0.90	0.70	Exponential	Mar	24.8	25.17	0.997	0.37	0.71	0.82	Ste

(*Continued.*)

Table 8 | Continued

Month	Est. T_{max}	Obr. T_{max}	RMSE	MBE	MAE	*r*	V.model	Month	Est. T_{max}	Obr. T_{max}	RMSE	MBE	MAE	*r*	V.model
Apr	24.54	24.70	1.08	0.15	0.93	0.66	Exponential	Apr	24.24	24.7	1.22	0.46	0.82	0.75	Ste
May	24.60	24.77	1.27	0.17	1.07	0.54	Exponential	May	24.18	24.77	1.56	0.60	1.02	0.64	Ste
Jun	23.03	23.17	1.59	0.14	1.34	0.27	Exponential	Jun	22.52	23.17	1.62	0.65	1.03	0.57	Ste
Jul	20.71	20.99	1.39	0.28	1.07	0.44	Exponential	Jul	20.36	20.99	1.62	0.63	1.03	0.580	Ste
Aug	20.21	20.51	1.29	0.30	0.97	0.49	Ste	Aug	19.93	20.51	1.52	0.58	0.98	0.59	Ste
Sep	21.58	21.69	1.36	0.10	1.24	0.47	Ste	Sep	21.12	21.69	1.44	0.57	0.96	0.68	Ste
Oct	22.75	22.89	1.03	0.13	0.93	0.72	Exponential	Oct	22.52	22.89	0.97	0.37	0.72	0.85	Ste
Nov	23.01	23.15	0.79	0.14	0.68	0.82	Ste	Nov	22.91	23.15	0.62	0.244	0.50	0.92	Ste
Dec	22.81	22.86	0.84	0.06	0.79	0.75	Exponential	Dec	22.62	22.86	0.62	0.24	0.46	0.91	Ste
Annual	23.09	23.20	1.16	0.11	1.04	0.59	Exponential	Annual	22.76	23.2	1.16	0.45	0.79	0.76	Ste

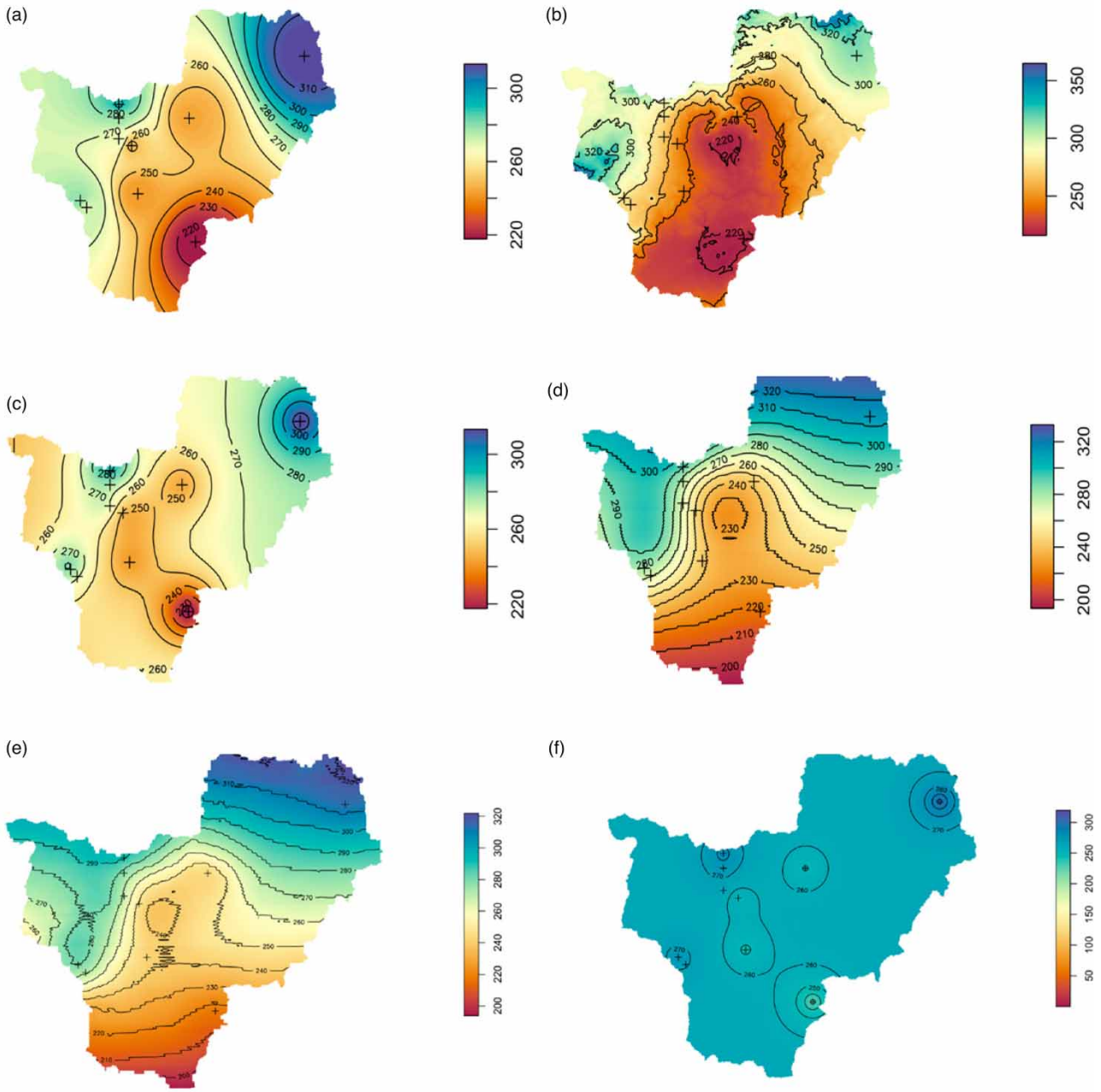

Figure 9 | Spatial map of 17 years August mean rainfall by (a) IDW, (b) KED 90 m DEM elevation, (c) KED with easting, (d) KED with northing, (e) KED with the combination of 90 m DEM and northing, and (f) OK.

easting as a covariate shows a high RMSE during the rainy season (June up to Sep). Therefore, based on the overall results shown in Table 7 and considering the rainy season, KED with northing as a covariate was selected as a suitable method for monthly interpolated rainfall datasets, and KED with elevation as a covariate was proven to be the best interpolation technique (in terms of errors but not *r*) selected for interpolating annual mean rainfall.

Table 8 depicts the descriptive statistical performance of the KED with various descriptors as covariates, IDW, and OK in terms of RMSE, MBE, MAE, and *r* for both the monthly and mean annual maximum temperature datasets. Based on the results shown in Table 8, KED with the combination of elevation and northing as a predictor shows the lowest statistical errors and the highest *r*-value compared to the rest of the interpolation techniques for most months and annually, followed by KED with elevation as a predictor. KED with easting as a covariate and OK relatively score the highest errors: RMSE,

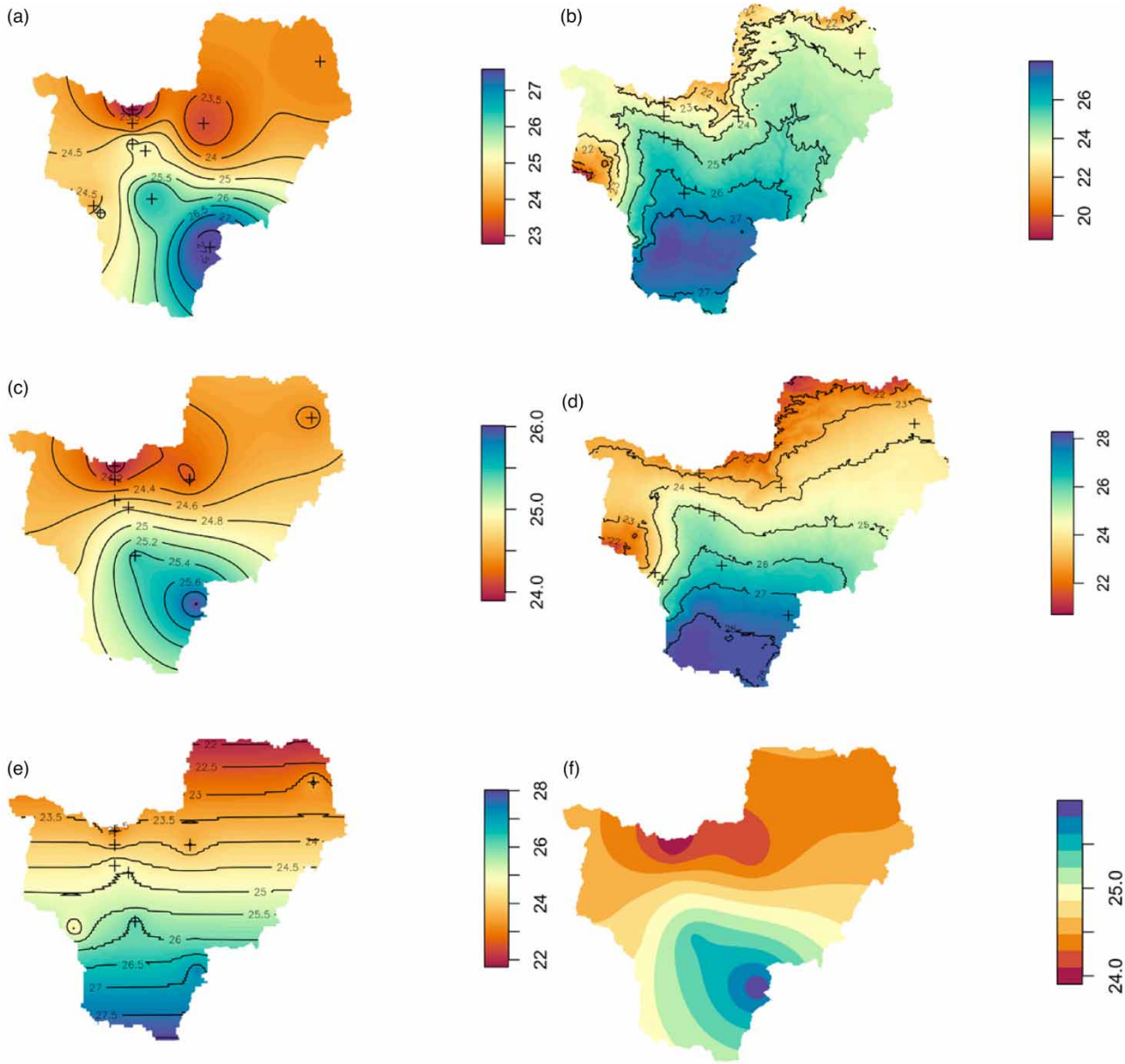

Figure 10 | Spatial map of 17 years April mean maximum temperature by (a) IDW, (b) KED with 90 m DEM elevation, (c) KED with easting, (d) KED with the combination of 90 m DEM elevation and northing, (e) KED with northing, and (f) OK.

MBE, and MAE on spatial prediction and mean monthly and annual maximum temperature estimation. As a result, KED with the combination of elevation and northing as a predictor was proven to be used as a suitable technique for the spatial prediction of the mean maximum temperature and the mean minimum temperature. The map shows that the spatial pattern of August mean rainfall, and April mean maximum temperature interpolated with various interpolation techniques, are displayed in Figures 9 and 10, respectively.

Figures 11 and 12 show the box plots of mean monthly rainfall using KED with northing as a predictor and mean minimum and maximum temperatures using KED with the combination of elevation and northing as a covariate for the Akaki catchment and for the Mille catchment using KED with a combination of elevation and easting as a covariate, respectively.

As observed from Figures 11 and 12 box plots, much higher scales plotting of climatic variable data were observed for the Mille catchment than the Akaki catchment, and the reason behind this was that both the estimated and actual climatic data were generally highly varying in the spatial pattern than Akaki's climatic variables. The bimodal nature of the rainfall pattern

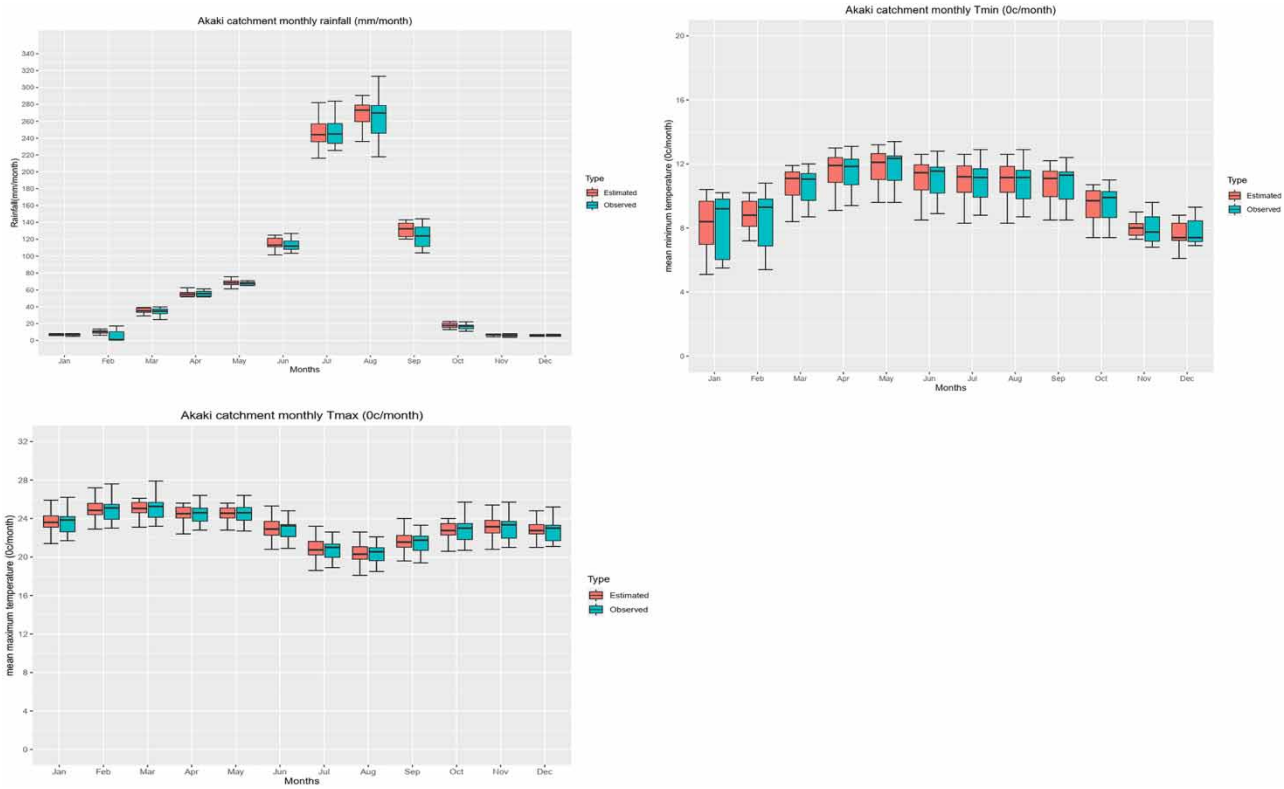

Figure 11 | Box plots for mean rainfall, T_{min}, and T_{max} for the Akaki catchment, obtained with KED.

was boldly observed in the Mille catchment, which was higher in the months of April and August than in the Akaki catchment. The maximum temperature was picked from February to May for the Akaki catchment, whereas it was picked approximately from March to July for the Mille catchment (see Figures 11 and 12). From careful inspection and prior knowledge of the authors, the KED with the combination of elevation and easting/northing as a covariate was generally acceptable in its predictive accuracy.

4. DISCUSSION

4.1. Spatial pattern of rainfall

Based on descriptive statistical evaluation parameters that the authors made (see subsection 3.2.), suitable interpolation techniques were selected for each spatial prediction of mean monthly and annual rainfall for Akaki and Mille catchments, respectively. The IDW and OK approaches resulted in the most constant zonal pattern of rainfall covering regions of different spatial elevations. In contrast, the KED method produced a spatial rainfall distribution that was closely related to the topography, and this was a result of the use of some external variables, namely elevation, easting, and northing, as the predictors (see Figures 7 and 9). The complex topographic relief influence on rainfall spatial distribution was more highly observed in the Mille catchment than in the Akaki catchment, and the reason for the latter catchment was that the catchment is comparatively flat but includes some higher elevation locations and areas such as the 'Intoto' mountain. Consequently, KED with various descriptors as a covariate (mentioned in Tables 5 and 7) was selected and performed to map the spatial mean monthly and annual rainfall.

The maps in Figures 7 and 9 depict that the spatial rainfall patterns and trends following the catchment's elevation trend were generally acceptable in their prediction reliability and accuracy. For instance, our obtained results showed that the spatial patterns by KED with northing as a covariate interpolated the mean monthly and annual rainfall gradually increase from south to north of the Akaki catchment (see Figure 9(d)) following the elevation increments, and for the Mille catchment from the east to the west (see Figure 7(f)) as catchment's elevation gradually increased using KED with the combination of

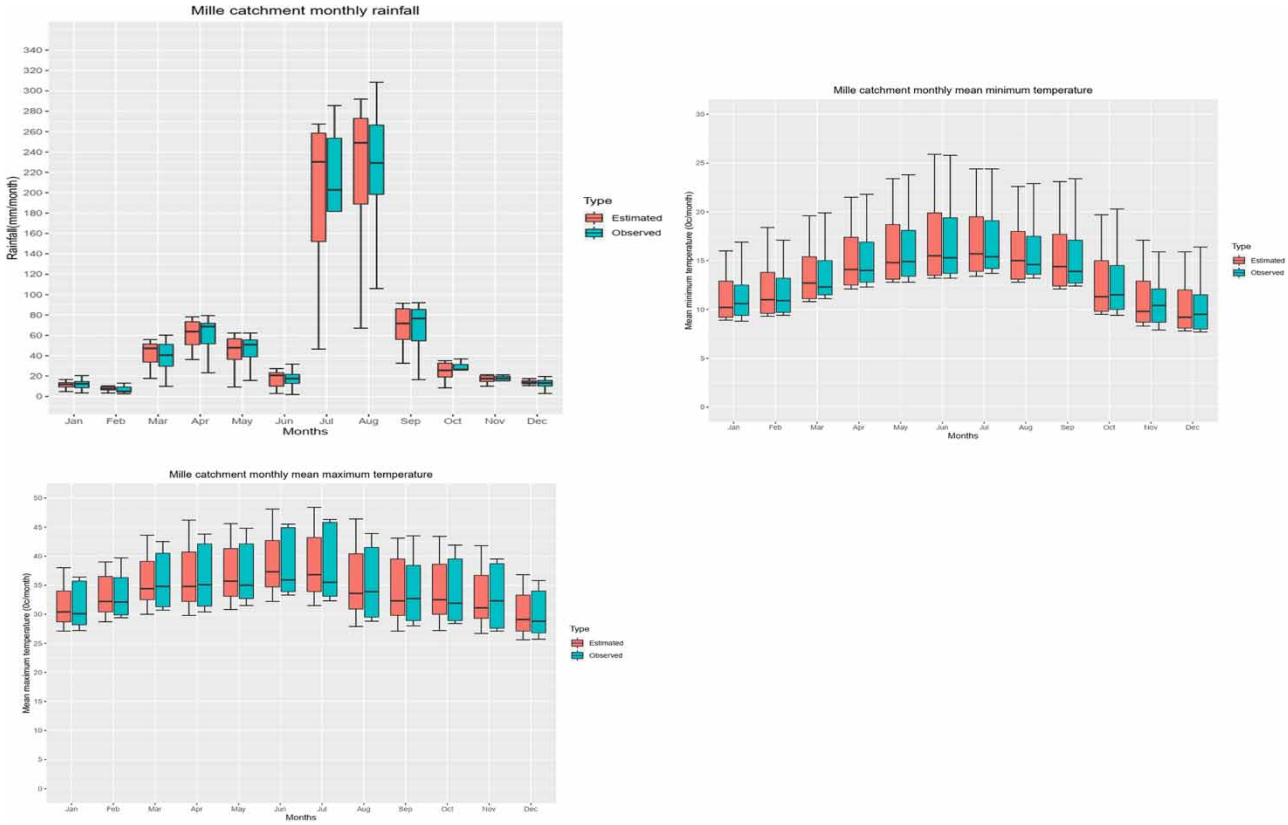

Figure 12 | Box plots for mean rainfall, T_{min}, and T_{max} for the Mille catchment, obtained with KED.

elevation and easting as a covariate. It is noted that the weakest correlation is between Mille's January rainfall and elevation because of the stronger correlations with the longitudinal location in summer.

The study by Goovaerts (2000) found that rainfall depths generally vary spatiotemporally and tend to increase with increasing elevations because of the orographic effect of mountainous terrain, which causes warm air to ascend vertically, and condensation occurs due to the adiabatic cooling effect. Havesi (1991) also discovered that there is a significant correlation between a natural log of average annual precipitation (AAP) and station elevation using a cokriging method with 62 rainfall stations in Nevada and southeastern California, which is similar to our obtained research findings, specifically for the Mille catchment. However, unlike the mille catchment, the spatial rainfall distribution in the Akaki catchment is less likely affected by orographic effects as well as longitudinal and/or latitudinal effects.

4.2. Spatial distribution of temperature

Similar to spatial rainfall but for temperature, the spatial interpolation techniques using KED with various covariates, IDW and OK, resulted in different spatial distributions of temperature (see Figures 8 and 10) for both the Mille and Akaki catchments. The OK and IDW methods resulted in the most gradual and smooth zonal patterns, while the KED with elevation, easting, and northing as covariates or with the combination of elevation and easting/northing as covariates showed an irregular distribution following the elevation trend; the temperature pattern exhibited a remarkable decrease with increasing elevation, and the research findings obtained by Matsuura (1995) exhibited the same results.

The spatial distribution of temperature determined by KED showed that the temperature gradually decreases from the east to the west for the Mille catchment (see Figure 8(c)–8(f)) and the south to the north for the Akaki catchment (see Figure 10(b)–10(e)). Accordingly, the spatial distribution of temperature produced by KED with the combination of elevation and easting (for the Mille catchment) and elevation and northing (for the Akaki catchment) as covariates exhibited better performance than the two unilateral interpolation techniques, IDW and OK, and they produced the most detailed and irregular spatial pattern compared with the results of the remaining techniques.

The principal contribution of this research resides in the covariate selection used in KED, and based on the proposed method, the selected predictors improved the predictive performance of KED. For instance, KED with the combination of either elevation and easting or elevation and northing as a predictor highly improves the prediction performance compared with KED with elevation, easting, or northing independently as a covariate (see Tables 5–8). Overall, from the results explained in sections 3 and 4, there were strong improvements in the spatial climatological variable prediction by using KED with the combination of elevation and easting/northing as a predictor.

5. CONCLUSIONS

As an important landscape descriptor, considering the combination of elevation and longitudinal/latitudinal location as a covariate in the spatial interpolation technique, especially in catchments with complex topography, is a key issue. Three interpolation techniques, i.e., two geostatistical techniques, OK and KED, and one deterministic interpolation technique, IDW, were described, and their performances were evaluated using cross-validation methodology. Among the geostatistical methods used in the estimation of the areal average climatological variables on both contrasting catchments, the KED approach incorporated secondary data, i.e. elevation, easting, and northing. Two univariate approaches, OK and IDW, served as benchmarks to which the multivariate approach, KED, could be compared to improve interpolation methods. The KED approach using auxiliary variables as a covariate exhibited significant improvement in interpolation accuracy and/or in reductions in interpolation error relative to unilateral interpolation methods, for example, OK and IDW. Among the KED approaches with a covariate, the one that combined DEM dataset (elevation) and the catchment's longitudinal location as a predictor performed the best, specifically for the Mille catchment. Therefore, it is clear that the incorporation of secondary data, as in our case study, can significantly minimize both the rainfall and temperature spatial interpolation errors for catchments with complex topography where climate stations are poor in terms of coverage and quality. Thus, it can be concluded that KED is identified as the best interpolation technique for the spatial interpolation of mean monthly and annual rainfall and temperature using the combination of elevation and easting/northing data as secondary information in both contrasting catchments, which is expected to be very useful in various climatological, hydrological, and water resource planning studies.

ACKNOWLEDGMENTS

The research was financed by the thesis and dissertation support fund through the Africa Center of Excellence for Water Management (ACEWM), Addis Ababa University, Ethiopia. We are also grateful to the Ethiopia National Meteorology Agency for providing the data and information used in this study. Additionally, the authors sincerely thank the Editor-in-Chief and the three anonymous reviewers for their constructive comments and valuable suggestions on the original version of the paper.

DATA AVAILABILITY STATEMENT

All relevant data are included in the paper or its Supplementary Information.

CONFLICT OF INTEREST

The authors declare there is no conflict.

REFERENCES

Adhikary, P. P. & Dash, C. J. 2017 Comparison of deterministic and stochastic methods to predict spatial variation of groundwater depth. *Applied Water Science* **7** (1), 339–348. https://doi.org/10.1007/s13201-014-0249-8.

Adhikary, S. K., Muttil, N. & Yilmaz, A. G. 2017 Cokriging for enhanced spatial interpolation of rainfall in two Australian catchments. *Hydrological Processes* **31** (12), 2143–2161. https://doi.org/10.1002/hyp.11163.

Amini, M. A., Torkan, G., Eslamian, S., Zareian, M. J. & Adamowski, J. F. 2019 Analysis of deterministic and geostatistical interpolation techniques for mapping meteorological variables at large watershed scales. *Acta Geophysica* **67** (1), 191–203. https://doi.org/10.1007/s11600-018-0226-y.

Bati, H. G. 2022 Digital elevation model resolution and its impact on the spatial pattern of rainfall-temperature prediction at the catchment scale: the case of the Mille catchment, Ethiopia. *Meteorology Hydrology and Water Management*. https://doi.org/10.26491/mhwm/149231.

Bertini, C., Buonora, L., Ridolfi, E., Russo, F. & Napolitano, F. 2020 On the use of satellite rainfall data to design a dam in an ungauged site. *Water (Switzerland)* **12** (11), 1–20. https://doi.org/10.3390/w12113028.

Cantet, P. 2017 Mapping the mean monthly precipitation of a small island using kriging with external drifts. *Theoretical and Applied Climatology* **127** (1–2), 31–44. https://doi.org/10.1007/s00704-015-1610-z.

Chen, F. & Li, X. 2016 Evaluation of IMERG and TRMM 3B43 monthly precipitation products over mainland China. *Remote Sensing* **8** (6), 1–18. https://doi.org/10.3390/rs8060472.

Chen, F. W. & Liu, C. W. 2012 Estimation of the spatial rainfall distribution using inverse distance weighting (IDW) in the middle of Taiwan. *Paddy and Water Environment* **10** (3), 209–222. https://doi.org/10.1007/s10333-012-0319-1.

Dinku, T. 2019 Challenges with availability and quality of climate data in Africa. *Extreme Hydrology and Climate Variability: Monitoring, Modelling, Adaptation and Mitigation* 71–80. https://doi.org/TT.

Dinku, T., Funk, C. & Grimes, D. 2008a The potential of satellite rainfall estimates for index insurance. *Earth* 1–5.

Dinku, T., Chidzambwa, S., Ceccato, P. & Connor, S. J. 2008b Validation of high-resolution satellite rainfall products over complex terrain. *International Journal of Remote Sensing* **29** (14), 4097–4110. https://doi.org/10.1080/01431160701772526.

Dinku, T., Thomson, M. C., Cousin, R., del Corral, J., Ceccato, P., Hansen, J. & Stephen, J. C. 2017 Enhancing National Climate Services (ENACTS) for development in Africa. *Climate and Development* **10** (7), 664–672. https://doi.org/10.1080/17565529.2017.1405784.

Di Piazza, A., Conti, F. L., Viola, F., Eccel, E. & Noto, L. V. 2015 Comparative analysis of spatial interpolation methods in the Mediterranean area: application to temperature in Sicily. *Water (Switzerland)* **7** (5), 1866–1888. https://doi.org/10.3390/w7051866.

Frazier, A. G., Giambelluca, T. W., Diaz, H. F. & Needham, H. L. 2016 Comparison of geostatistical approaches to spatially interpolate month-year rainfall for the Hawaiian Islands. *International Journal of Climatology* **36** (3), 1459–1470. https://doi.org/10.1002/joc.4437.

Gebere, S. B., Alamirew, T., Merkel, B. J. & Melesse, A. M. 2015 Performance of high resolution satellite rainfall products over data scarce parts of eastern Ethiopia. *Remote Sensing* **7** (9), 11639–11663. https://doi.org/10.3390/rs70911639.

Gebremedhin, M. A., Lubczynski, M. W., Maathuis, B. H. P. & Teka, D. 2021 Novel approach to integrate daily satellite rainfall with in-situ rainfall, Upper Tekeze Basin, Ethiopia. *Atmospheric Research* **248**, 105135. https://doi.org/10.1016/j.atmosres.2020.105135.

Gebremichael, M. & Hossain, F. 2010 Satellite rainfall applications for surface hydrology. *Satellite Rainfall Applications for Surface Hydrology* 1–327. https://doi.org/10.1007/978-90-481-2915-7.

Goovaerts, P. 1997 *Geostatistics for Natural Resources Evaluation*.

Goovaerts, P. 2000 Geostatistical approaches for incorporating elevation into the spatial interpolation of rainfall. *Journal of Hydrology* **228** (1–2), 113–129. https://doi.org/10.1016/S0022-1694(00)00144-X.

Grimes, D. I. F., Pardo-Igúzquiza, E. & Bonifacio, R. 1999 Optimal areal rainfall estimation using raingauges and satellite data. *Journal of Hydrology* **222** (1–4), 93–108. https://doi.org/10.1016/S0022-1694(99)00092-X.

Haberlandt, U. 2007 Geostatistical interpolation of hourly precipitation from rain gauges and radar for a large-scale extreme rainfall event. *Journal of Hydrology* **332** (1–2), 144–157. https://doi.org/10.1016/j.jhydrol.2006.06.028.

Havesi, J. A. 1991 Precipitation Estimation in Mountainous Using Multivariate Geostatistics. Part I: Structural Analysis. *Journal of Applied Meteorology* **31** (7), 661–676.

Hudson, G. & Wackernagel, H. 1994 Mapping temperature using kriging with external drift: theory and an example from Scotland. *International Journal of Climatology* **14** (1), 77–91. https://doi.org/10.1002/joc.3370140107.

Isaaks, E. H. 1990 Applied geostatistics. *Choice Reviews Online* **28** (01). https://doi.org/10.5860/choice.28-0304.

Isaaks, E. H. & Srivastava, R. M. 1989 An introduction to applied geostatistics. In: *Geographical Analysis*, Vol. 26, 3, pp. 282–283. https://doi.org/10.1111/j.1538-4632.1994.tb00325.x.

Jalili Pirani, F. & Modarres, R. 2020 Geostatistical and deterministic methods for rainfall interpolation in the Zayandeh Rud basin, Iran. *Hydrological Sciences Journal* **65** (16), 2678–2692. https://doi.org/10.1080/02626667.2020.1833014.

Kaufman, C. G. & Shaby, B. A. 2013 The role of the range parameter for estimation and prediction in geostatistics. *Biometrika* **100** (2), 473–484. https://doi.org/10.1093/biomet/ass079.

Kisaka, M. O., Mucheru-Muna, M., Ngetich, F. K., Mugwe, J., Mugendi, D., Mairura, F., Shisanya, C. & Makokha, G. L. 2016 Potential of deterministic and geostatistical rainfall interpolation under high rainfall variability and dry spells: case of Kenya's Central Highlands. *Theoretical and Applied Climatology* **124** (1–2), 349–364. https://doi.org/10.1007/s00704-015-1413-2.

Lebel, T., Bastin, G., Obled, C. & Creutin, J. D. 1987 On the accuracy of areal rainfall estimation: a case study. *Water Resources Research* **23** (11), 2123–2134. https://doi.org/10.1029/WR023i011p02123.

Le Coz, C. & Van De Giesen, N. 2020 Comparison of rainfall products over sub-saharan Africa. *Journal of Hydrometeorology* **21** (4), 553–596. https://doi.org/10.1175/JHM-D-18-0256.1.

Li, J. & Heap, A. D. 2008 A review of spatial interpolation methods for environmental scientists. In: *Australian Geological Survey Organisation, GeoCat# 68(2008/23)*. p. 154. https://doi.org/http://www.ga.gov.au/image_cache/GA12526.pdf.

Lloyd, C. D. 2005 Assessing the effect of integrating elevation data into the estimation of monthly precipitation in Great Britain. *Journal of Hydrology* **308** (1–4), 128–150. https://doi.org/10.1016/j.jhydrol.2004.10.026.

Lu, S., Veldhuis, M. C. T. & Van De Giesen, N. 2020 A methodology for multiobjective evaluation of precipitation products for extreme weather (In a data-scarce environment). *Journal of Hydrometeorology* **21** (6), 1223–1244. https://doi.org/10.1175/JHM-D-19-0157.1.

Ly, S., Charles, C. & Degr, A. 2011 *Geostatistical Interpolation of Daily Rainfall at Catchment Scale: the Use of Several Variogram Models in the Ourthe and Ambleve Catchments, Belgium*, pp. 2259–2274. https://doi.org/10.5194/hess-15-2259-2011.

Matsuura, C. J. W. A. K. 1995 *Smart Interpolation of Annually Air Temperature in the United States*. American Meteorological Society, Boston, MA.

Ministry of Water Resources 2009 *Federal Democratic Republic of Ethiopia Ministry of Water Resources Mille and Dirma Integrated Sub-Watershed Management Study Annex A: Climate and Water Resources (Final)*.

Molla, D., Stefan, W., Gizaw, B. & Stichler, W. 2005 Groundwater recharge in the Akaki catchment, central Ethiopia: evidence from environmental isotopes (d18O, d2H and 3H) and chloride mass balance. **2274** (November 2008), 2267–2274. https://doi.org/10.1002/hyp.

Mukhopadhaya, S. 2016 Rainfall mapping using ordinary kriging technique: case study: Tunisia. *Journal of Basic and Applied Engineering Research*. **3** (1), 1–5.

Nalder, I. A. & Wein, R. W. 1998 Spatial interpolation of climatic Normals: test of a new method in the Canadian boreal forest. *Agricultural and Forest Meteorology* **92** (4), 211–225. https://doi.org/10.1016/S0168-1923(98)00102-6.

Novikov, S. L. 1981 Elevation: a major influence on the hydrology of New Hampshire and Vermont, USA. *Hydrological Sciences Bulletin* **26** (4), 399–413. https://doi.org/10.1080/02626668109490904.

Otieno, H., Yang, J., Liu, W. & Han, D. 2014 Influence of rain gauge density on interpolation method selection. *Journal of Hydrologic Engineering* **19** (11), 04014024. https://doi.org/10.1061/(asce)he.1943-5584.0000964.

Parker, D., Good, E. & Chadwick, R. 2011 Reviews of observational data available over Africa for monitoring, attribution and forecast evaluation. *Hadley Centre Technical Note* **86** (June), 1–63.

Pebesma, E. J. 2003 Gstat: multivariable geostatistics for S. Dsc. In: *Proceedings of DSC* (Hornik, K., Leisch, F. & Zeileis, A., eds.), March 20–22, 2003, Vienna, Austria.

Pebesma, E. J. 2004 Multivariable geostatistics in S: the gstat package. *Computers and Geosciences* **30** (7), 683–691. https://doi.org/10.1016/j.cageo.2004.03.012.

Pebesma, E. 2012 Spacetime: spatio-temporal data in R. *Journal of statistical software* **51**, 1–30.

Pebesma, E. J. & Wesseling, C. G. 1998 GSTAT: a program for geostatistical modelling, prediction and simulation. *Computers & Geosciences* **24** (1), 17–31.

Petković, V. & Kummerow, C. D. 2017 Understanding the sources of satellite passive microwave rainfall retrieval systematic errors over land. *Journal of Applied Meteorology and Climatology* **56** (3), 597–614. https://doi.org/10.1175/JAMC-D-16-0174.1.

Phillips, D. L., Dolph, J. & Marks, D. 1992 A comparison of geostatistical procedures for spatial analysis of precipitation in mountainous terrain. *Agricultural and Forest Meteorology* **58** (1–2), 119–141. https://doi.org/10.1016/0168-1923(92)90114-J.

Rata, M., Douaoui, A., Larid, M. & Douaik, A. 2020 Comparison of geostatistical interpolation methods to map annual rainfall in the Chéliff watershed, Algeria. *Theoretical and Applied Climatology* **141** (3–4), 1009–1024. https://doi.org/10.1007/s00704-020-03218-z.

Rossiter, D. G. 2014 *Applied Geostatistics Exercise 5b: Predicting From Point Samples (Part 4) Lognormal Kriging*. Part 4, University of Twente, Faculty of Geo-Information Science & Earth Observation (ITC), Enschede, Netherlands.

Shepard, D. 1968 *A Two-Dimensional Interpolation Function for Irregularly-Spaced Data*. Proceedings of the 1968 ACM National Conference, New York, 27-29 August 1968, 517–524. http://dx.doi.org/10.1145/800186.810616.

Stein, M. 2010 *Asymptotics for Spatial Processes*. https://doi.org/10.1201/9781420072884-c6.

Taesombat, W. & Sriwongsitanon, N. 2009 Areal rainfall estimation using spatial interpolation techniques. *ScienceAsia* **35** (3), 268–275. https://doi.org/10.2306/scienceasia1513-1874.2009.35.268.

Tas, E. & Taş, E. 2017 Comparison of monthly TRMM and ground-based precipitation data in Akarcay Basin, Turkey. In: *8th Atmospheric Sciences Symposium*, December.

Toté, C., Patricio, D., Boogaard, H., van der Wijngaart, R., Tarnavsky, E. & Funk, C. 2015 Evaluation of satellite rainfall estimates for drought and flood monitoring in Mozambique. *Remote Sensing* **7** (2), 1758–1776. https://doi.org/10.3390/rs70201758.

Vicente-Serrano, S. M., Saz-Sánchez, M. A. & Cuadrat, J. M. 2003 Comparative analysis of interpolation methods in the middle Ebro Valley (Spain): application to annual precipitation and temperature. *Climate Research* **24** (2), 161–180. https://doi.org/10.3354/cr024161.

Wackernagel, H. 1998 *Multivariate Geostatistics: An Introduction with Applications*, Vol. 148. Kluwer Academic Publishers, the Netherlands.

Wackernagel, H. 2003 *Multivariate Geostatistics: an Introduction with Applications (Third, com, Vol. 148)*. Kluwer Aeademic Publishers, The Netherlands.

Washington, R., Harrison, M., Conway, D., Black, E., Challinor, A., Grimes, D., Jones, R., Morse, A., Kay, G. & Todd, M. 2006 African climate change: taking the shorter route. *Bulletin of the American Meteorological Society* **87** (10), 1355–1366. https://doi.org/10.1175/BAMS-87-10-1355.

Webster, R. & Oliver, M. 2007 Geostatistics for environmental scientists. *Vadose Zone Journal* **1** (2). https://doi.org/10.2136/vzj2002.3210.

Wilson, J. P., Spangrud, D. J., Nielsen, G. A., Jacobsen, J. S. & Tyler, D. A. 1998 Global positioning system sampling intensity and pattern effects on computed topographic attributes. *Soil Science Society of America Journal* **62** (5), 1410–1417.

Yang, Z., Hsu, K., Sorooshian, S., Xu, X., Braithwaite, D., Zhang, Y. & Verbist, K. M. J. 2017 Merging high-resolution satellite-based precipitation fields and point-scale rain gauge measurements – a case study in Chile. *Journal of Geophysical Research* **122** (10), 5267–5284. https://doi.org/10.1002/2016JD026177.

First received 25 February 2022; accepted in revised form 30 June 2022. Available online 20 July 2022